Online-PDH©

Online Continuing Education for Professional Engineers
Since 2009

Molten Carbonate Fuel Cells

PDH Credits:
4 PDH

Course No.:
MFC101

Publication Source:
US Dept. of Energy
"Fuel Cell Handbook", Chapter 6

Release Date:
2002

1265 San Juan Dr. - Merritt Island, FL 32952
Phone: 321-501-5601

6. MOLTEN CARBONATE FUEL CELL

The molten carbonate fuel cell operates at approximately 650 °C (1200 °F). The high operating temperature is needed to achieve sufficient conductivity of the carbonate electrolyte, yet allow the use of low-cost metal cell components. A benefit associated with this high temperature is that noble metal catalysts are not required for the cell electrochemical oxidation and reduction processes. Molten carbonate fuel cells are being developed for natural gas and coal-based power plants for industrial, electrical utility, and military applications[19]. Currently, one industrial corporation is actively pursuing the commercialization of MCFCs in the U.S.: FuelCell Energy (FCE). Europe and Japan each have at least one developer pursuing the technology: MTU Friedrichshafen, Ansaldo (Italy), and Ishikawajima-Harima Heavy Industries (Japan).

Figure 6-1 depicts the operating configuration of the molten carbonate fuel cell. The half cell electrochemical reactions are

$$H_2 + CO_3^{=} \rightarrow H_2O + CO_2 + 2e^- \qquad (6\text{-}1)$$

at the anode, and

$$½O_2 + CO_2 + 2e^- \rightarrow CO_3^{=} \qquad (6\text{-}2)$$

at the cathode. The overall cell reaction[20] is

$$H_2 + ½O_2 + CO_2 \text{ (cathode)} \rightarrow H_2O + CO_2 \text{ (anode)} \qquad (6\text{-}3)$$

[19]. MCFCs operate more efficiently with CO_2 containing bio-fuel derived gases. Performance loss on the anode due to fuel dilution is compensated by cathode side performance enhancement resulting from CO_2 enrichment.

[20]. CO is not directly used by electrochemical oxidation, but produces additional H_2 when combined with water in the water gas shift reaction.

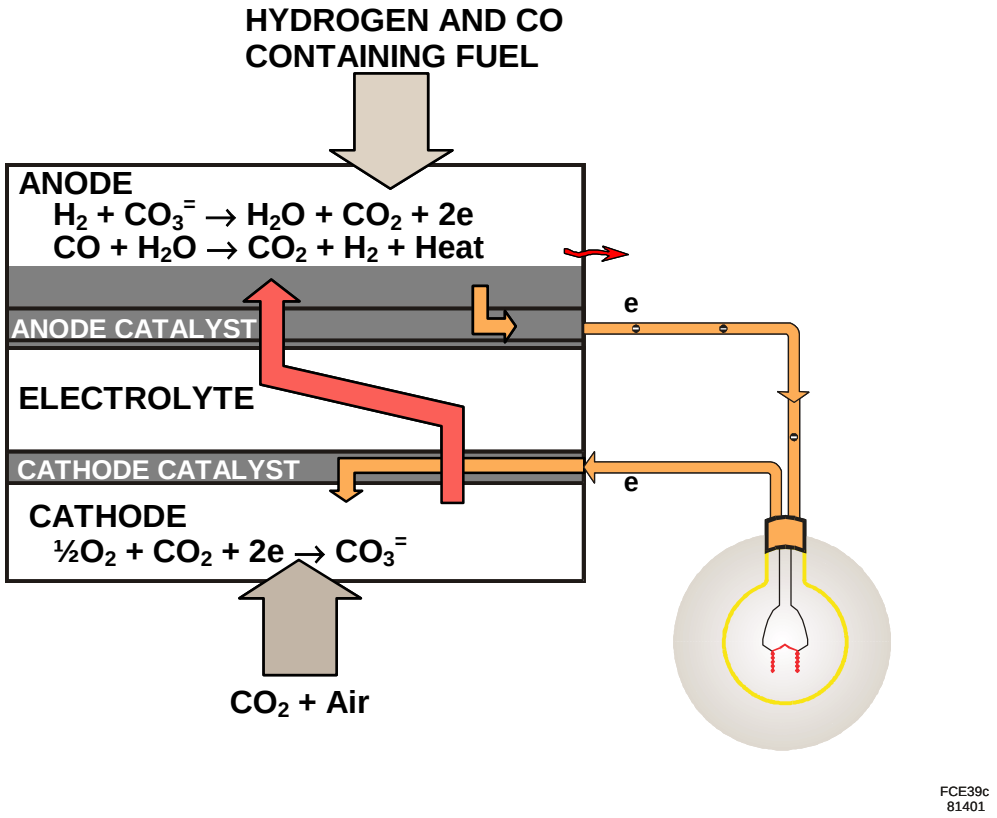

Figure 6-1 Principles of Operation of Molten Carbonate Fuel Cells (FuelCell Energy)

Besides the reaction involving H_2 and O_2 to produce H_2O, Equation 6-3 shows a transfer of CO_2 from the cathode gas stream to the anode gas stream via the $CO_3^{=}$ ion, with 1 mole CO_2 transferred along with two Faradays of charge, or 2 gram moles of electrons. The reversible potential for an MCFC, taking into account the transfer of CO_2, is given by the equation

$$E = E^\circ + \frac{RT}{2F} \ln \frac{P_{H_2} P_{O_2}^{1/2}}{P_{H_2O}} + \frac{RT}{2F} \ln \frac{P_{CO_{2,c}}}{P_{CO_{2,a}}} \qquad (6\text{-}4)$$

where the subscripts a and c refer to the anode and cathode gas compartments, respectively. When the partial pressures of CO_2 are identical at the anode and cathode, and the electrolyte is invariant, the cell potential depends only on the partial pressures of H_2, O_2, and H_2O. Typically, the CO_2 partial pressures are different in the two electrode compartments and the cell potential is affected accordingly.

The need for CO_2 at the cathode requires some schemes that will either 1) transfer the CO_2 from the anode exit gas to the cathode inlet gas ("CO_2 transfer device"), 2) produce CO_2 by combusting the anode exhaust gas, which is mixed directly with the cathode inlet gas, or 3) supply CO_2 from an

alternate source. It is usual practice in an MCFC system that the CO_2 generated at the anode (right side of Equation 6-1) be routed (external to the cell) to the cathode (left side of Equation 6-2).

MCFCs differ in many respects from PAFCs because of their higher operating temperature (650 vs. 200 °C) and the nature of the electrolyte. The higher operating temperature of MCFCs provides the opportunity to achieve higher overall system efficiencies (potential for heat rates below 7,500 Btu/kWh) and greater flexibility in the use of available fuels.[21] On the other hand, the higher operating temperature places severe demands on the corrosion stability and life of cell components, particularly in the aggressive environment of the molten carbonate electrolyte. Another difference between PAFCs and MCFCs lies in the method used for electrolyte management in the respective cells. In a PAFC, PTFE serves as a binder and wet-proofing agent to maintain the integrity of the electrode structure and to establish a stable electrolyte/gas interface in the porous electrode. The phosphoric acid is retained in a matrix of PTFE and SiC between the anode and cathode. There are no high temperature, wetproofing materials available for use in MCFCs that are comparable to PTFE. Thus, a different approach is required to establish a stable electrolyte/gas interface in MCFC porous electrodes, and this is illustrated schematically in Figure 6-2. The MCFC relies on a balance in capillary pressures to establish the electrolyte interfacial boundaries in the porous electrodes (1, 2, 3). At thermodynamic equilibrium, the diameters of the largest flooded pores in the porous components are related by the equation

$$\frac{\gamma_c \cos\theta_c}{D_c} = \frac{\gamma_e \cos\theta_e}{D_e} = \frac{\gamma_a \cos\theta_a}{D_a} \qquad (6\text{-}5)$$

where γ is the interfacial surface tension, θ is the contact angle of the electrolyte, D is the pore diameter, and the subscripts a, c, and e refer to the anode, cathode and electrolyte matrix, respectively. By properly coordinating the pore diameters in the electrodes with those of the electrolyte matrix, which contains the smallest pores, the electrolyte distribution depicted in Figure 6-2 is established. This arrangement permits the electrolyte matrix to remain completely filled with molten carbonate, while the porous electrodes are partially filled, depending on their pore size distributions. According to the model illustrated in Figure 6-2 and described by Equation (6-5), the electrolyte content in each of the porous components will be determined by the equilibrium pore size (<D>) in that component; pores smaller than <D> will be filled with electrolyte, and pores larger than <D> will remain empty. A reasonable estimate of the volume distribution of electrolyte in the various cell components is obtained from the measured pore-volume-distribution curves and the above relationship for D (1, 2).

Electrolyte management, that is, control over the optimum distribution of molten carbonate electrolyte in the different cell components, is critical for achieving high performance and endurance with MCFCs. Various processes (i.e., consumption by corrosion reactions, potential-driven migration, creepage of salt and salt vaporization) occur, all of which contribute to the redistribution of molten carbonate in MCFCs; these aspects are discussed by Maru, et al. (4) and Kunz (5).

[21]. *In situ* reforming of fuels in MCFCs is possible as discussed later in the section.

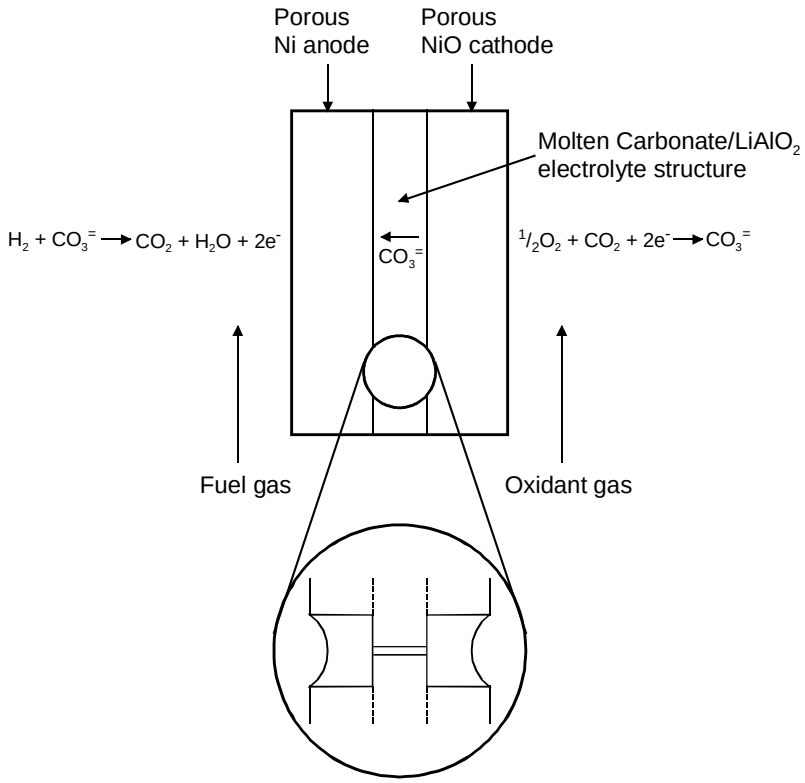

Figure 6-2 Dynamic Equilibrium in Porous MCFC Cell Elements
(Porous electrodes are depicted with pores covered by a thin film of electrolyte)

6.1 Cell Components

6.1.1 State-of-the-Art Componments

The data in Table 6-1 provide a chronology of the evolution in MCFC component technology. In the mid-1960s, electrode materials were, in many cases, precious metals, but the technology soon evolved to use Ni-based alloys at the anode and oxides at the cathode. Since the mid-1970s, the materials for the electrodes and electrolyte (molten carbonate/$LiAlO_2$) have remained essentially unchanged. A major development in the 1980s was the evolution in fabrication of electrolyte structures. Developments in cell components for MCFCs have been reviewed by Maru, et al. (6, 7), Petri and Benjamin (8), and Selman (9). Over the past 28 years, the performance of single cells has improved from about 10 mW/cm^2 to >150 mW/cm^2. During the 1980s, both the performance and endurance of MCFC stacks dramatically improved. The data in Figure 6-3 illustrate the progress that has been made in the performance of single cells, and in the cell voltage of small stacks at 650 °C. Several MCFC stack developers have produced cell stacks with cell areas up to 1 m^2. Tall, full-scale U.S. stacks fabricated to date include several FCE-300 plus cell stacks with ~9000 cm^2 cell area producing >250 kW.

Table 6-1 Evolution of Cell Component Technology for Molten Carbonate Fuel Cells

Component	Ca. 1965	Ca. 1975	Current Status
Anode	• Pt, Pd, or Ni	• Ni-10 Cr	• Ni-Cr/Ni-Al/Ni-Al-Cr • 3-6 μm pore size • 45 to 70 percent initial porosity • 0.20 to .5 mm thickness • 0.1 to1 m^2/g
Cathode	• Ag_2O or lithiated NiO	• lithiated NiO	• lithiated NiO-MgO • 7 to15 μm pore size • 70 to 80 percent initial porosity • 60 to 65 percent after lithiation and oxidation • 0.5 to 1 mm thickness • 0.5 m^2/g
Electrolyte Support	• MgO	• mixture of α-, β-, and γ-$LiAlO_2$ • 10 to 20 m^2/g • 1.8 mm thickness	• γ-$LiAlO_2$, α-$LiAlO_2$ • 0.1 to12 m^2/g • 0.5 to1 mm thickness
Electrolyte[a] (wt percent)	• 52 Li-48 Na • 43.5 Li-31.5 Na-25 K • "paste"	• 62 Li-38 K • hot press "tile" • 1.8 mm thickness	• 62 Li-38 K • 60 Li-40 Na 51 Li-48 Na • tape cast • 0.5 to1 mm thickness

a - Mole percent of alkali carbonate salt

Specifications for the anode and cathode were obtained from References (6), (10), and (11).

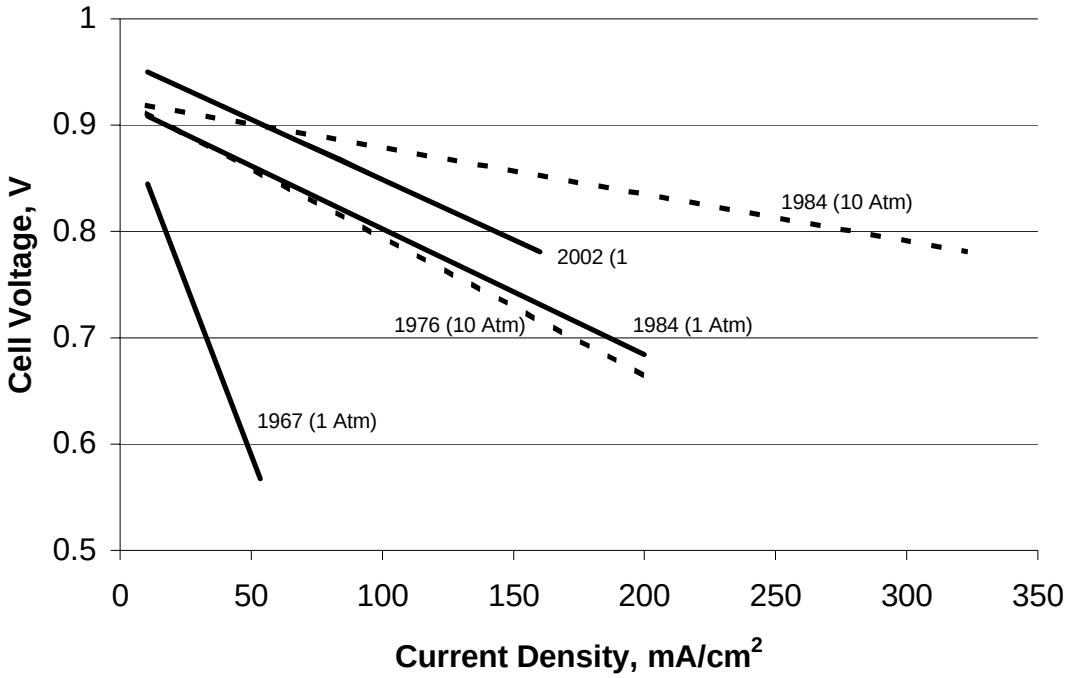

Figure 6-3 Progress in the Generic Performance of MCFCs on Reformate Gas and Air (12, 13)

The conventional process to fabricate electrolyte structures until about 1980 involved hot pressing (about 5,000 psi) mixtures of $LiAlO_2$ and alkali carbonates (typically >50 vol percent in liquid state) at temperatures slightly below the melting point of the carbonate salts (e.g., 490°C for electrolyte containing 62 mol Li_2CO_3-38 mol K_2CO_3). These electrolyte structures (also called "electrolyte tiles") were relatively thick (1 to 2 mm) and difficult to produce in large sizes[22] because large tooling and presses were required. The electrolyte structures produced by hot pressing are often characterized by 1) void spaces (<5 porosity), 2) poor uniformity of microstructure, 3) generally poor mechanical strength, and 4) high iR drop. To overcome these shortcomings of hot pressed electrolyte structures, alternative processes such as tape casting (7) and electrophoretic deposition (14) for fabricating thin electrolyte structures were developed. The greatest success to date with an alternative process has been reported with tape casting, which is a common processing technique used by the ceramics industry. This process involves dispersing the ceramic powder in a solvent[23] that contains dissolved binders (usually an organic compound), plasticizers, and additives to yield the proper slip rheology. The slip is cast over a moving smooth substrate, and the desired thickness is established with a doctor blade device. After drying the slip, the "green" structure is assembled into the fuel cell where the organic binder is removed by thermal decomposition, and the absorption of alkali carbonate into the ceramic structure occurs during cell startup.

[22]. The largest electrolyte tile produced by hot pressing was about 1.5 m^2 in area (7).
[23]. An organic solvent is used because $LiAlO_2$ in the slip reacts with H_2O.

The tape casting and electrophoretic deposition processes are amenable to scale-up, and thin electrolyte structures (0.25-0.5 mm) can be produced. The ohmic resistance of an electrolyte structure[24] and the resulting ohmic polarization have a large influence on the operating voltage of MCFCs (15). FCE has stated that the electrolyte matrix encompasses 70 of the ohmic loss (16) of the cell. At a current density of 160 mA/cm^2, the voltage drop (ΔV_{ohm}) of an 0.18 cm thick electrolyte structure, with a specific conductivity of ~0.3/ohm-cm at 650 °C, was found to obey the relationship (14),

$$\Delta V_{ohm}\,(V) = 0.5t \qquad (6\text{-}6)$$

where ΔV_{ohm} is in volts and t is the thickness in cm. Later data confirm this result (16). With this equation, it is apparent that a fuel cell with an electrolyte structure of 0.25 cm thickness would operate at a cell voltage that is 35 mV higher than that of an identical cell with an electrolyte structure of 0.18 cm thickness because of the lower ohmic loss. Thus, there is a strong incentive for making thinner electrolyte structures to improve cell performance.

The electrolyte composition affects the performance and endurance of MCFCs in several ways. Higher ionic conductivities, and hence lower ohmic polarization, are achieved with Li-rich electrolytes because of the relative high ionic conductivity of Li_2CO_3 compared to that of Na_2CO_3 and K_2CO_3. However, gas solubility and diffusivity are lower, and corrosion is more rapid in Li_2CO_3.

The major considerations with Ni-based anodes and NiO cathodes are structural stability and NiO dissolution, respectively (9). Sintering and mechanical deformation of the porous Ni-based anode under compressive load lead to performance decay by redistribution of electrolyte in a MCFC stack. The dissolution of NiO in molten carbonate electrolyte became evident when thin electrolyte structures were used. Despite the low solubility of NiO in carbonate electrolytes (~10 ppm), Ni ions diffuse in the electrolyte towards the anode, and metallic Ni can precipitate in regions where a H_2 reducing environment is encountered. The precipitation of Ni provides a sink for Ni ions, and thus promotes the diffusion of dissolved Ni from the cathode. This phenomenon becomes worse at high CO_2 partial pressures (17, 18) because dissolution may involve the following mechanism:

$$NiO + CO_2 \rightarrow Ni^{2+} + CO^{=}_3 \qquad (6\text{-}7)$$

The dissolution of NiO has been correlated to the acid/base properties of the molten carbonate. The basicity of the molten carbonate is defined as equal to -log (activity of $O^{=}$) or -log a_{M_2O}, where a is the activity of the alkali metal oxide M_2O. Based on this definition, acidic oxides are associated with carbonates (e.g., K_2CO_3) that do not dissociate to M_2O, and basic oxides are formed with highly dissociated carbonate salts (e.g., Li_2CO_3). The solubility of NiO in binary

[24]. Electrolyte structures containing 45 wt% $LiAlO_2$ and 55 wt% molten carbonate (62 mol% Li_2CO_3-38 mol% K_2CO_3) have a specific conductivity at 650°C of about 1/3 that of the pure carbonate phase (15).

carbonate melts shows a clear dependence on the acidity/basicity of the melt (19, 20). In relatively acidic melts, NiO dissolution can be expressed by

$$NiO \rightarrow Ni^{2+} + O^{=} \qquad (6\text{-}8)$$

In basic melts, NiO reacts with $O^{=}$ to produce one of two forms of nickelate ions:

$$NiO + O^{=} \rightarrow NiO_2^{=} \qquad (6\text{-}9)$$

$$2NiO + O^{=} + \tfrac{1}{2}O_2 \rightarrow 2NiO_2^{-} \qquad (6\text{-}10)$$

A distinct minimum in NiO solubility is observed in plots of log (NiO solubility) versus basicity (-log a_{M_2O}), which can be demarcated into two branches corresponding to acidic and basic dissolution. Acidic dissolution is represented by a straight line with a slope of +1, and a NiO solubility that decreases with an increase in a_{M_2O}. Basic dissolution is represented by a straight line with a slope of either -1 or -½, corresponding to Equations (6-9) and (6-10), respectively. The CO_2 partial pressure is an important parameter in the dissolution of NiO in carbonate melts because the basicity is directly proportional to log P_{CO_2}. An MCFC usually operates with a molten carbonate electrolyte that is acidic.

Based on a 12,000-hour full-size stack tests as well as post-test results, FCE believes that Ni dissolution and subsequent precipitation will not be an issue for the desired 40,000-hour (5-yr) life (21) at atmospheric pressure. But at 10 atm cell pressure, only about 5,000 to 10,000 hours may be possible with currently available NiO cathodes (22). The solubility of NiO in molten carbonates is complicated by its dependence on several parameters: carbonate composition, H_2O partial pressure, CO_2 partial pressure, and temperature. For example, measurements of NiO dissolution by Kaun (23) indicate that solubility is affected by changing the electrolyte composition; a lower solubility is obtained in a Li_2CO_3-K_2CO_3 electrolyte that contains less Li_2CO_3 (i.e., lower solubility in 38 mol Li_2CO_3-62 mol K_2CO_3 than in 62 mol Li_2CO_3-38 mol K_2CO_3 at 650 °C). However, the solubility of Ni increases in the electrolyte with 38 mol Li_2CO_3 when the temperature decreases, whereas the opposite trend is observed in the electrolyte with 62 mol Li_2CO_3. Another study reported by Appleby (24) indicates that the solubility of Ni decreases from 9 to 2 ppm by increasing the Li concentration in Li_2CO_3-K_3CO_3 from 62 to 75 wt percent, and a lower solubility is obtained in 60 mol percent Li_2CO_3-40 mol percent Na_2CO_3 at 650 °C. The compaction of cathodes became evident in MCFC stacks once the anode creep was eliminated when strengthened by oxide dispersion [i.e., oxide dispersion strengthened (ODS) anode].

The bipolar plates used in MCFC stacks are usually fabricated from thin (~15 mil) sheets of an alloy (e.g., Incoloy 825, 310S or 316L stainless steel) that are coated on one side (i.e., the side

exposed to fuel gases in the anode compartment) with a Ni layer. The Ni layer is stable in the reducing gas environment of the anode compartment, and it provides a conductive surface coating with low contact resistance. Pigeaud, et al. describe approaches to circumvent the problems associated with gas leaks and corrosion of bipolar plates (25). Corrosion is largely overcome by applying a coating (about 50 μm thickness) at the vulnerable locations on the bipolar plate. For example, the wet-seal[25] area on the anode side is subject to a high chemical potential gradient because of the fuel gas inside the cell and the ambient environment (usually air) on the outside of the cell, which promotes corrosion (about two orders of magnitude greater than in the cathode wet-seal area (26)). Donado, et al. present a general discussion on corrosion in the wet-seal area of MCFCs (27). A thin aluminum coating in the wet-seal area of a bipolar plate provides corrosion protection by forming a protective layer of $LiAlO_2$ after reaction of Al with Li_2CO_3 (28). Such a protective layer would not be useful in areas of the bipolar plate that must permit electronic conduction because $LiAlO_2$ is an insulating material.

A dense and electronically insulating layer of $LiAlO_2$ is not suitable for providing corrosion resistance to the cell current collectors because these components must remain electrically conductive. The typical materials used for this application are 316 stainless steel and Ni plated stainless steels. However, materials with better corrosion resistance are required for long-term operation of MCFCs. Research is continuing to understand the corrosion processes of high-temperature alloys in molten carbonate salts under both fuel gas and oxidizing gas environments (29, 28) and to identify improved alloys (30) for MCFCs. Stainless steels such as Type 310 and 446 have demonstrated better corrosion resistance than Type 316 in corrosion tests (30).

6.1.2 Development Components

MCFC components are limited by several technical considerations (31), particularly those described in Section 6.1.1. Even though present approaches function properly in full size cells at atmospheric pressure, research is addressing alternate cathode materials and electrolytes, performance improvement, life extension beyond the commercialization goal of five years, and cost reduction (32). The studies described in recent literature provide updated information on promising development of the electrodes, the electrolyte matrix, and the capability of the cell to tolerate trace contaminants in the fuel supply. Descriptions of some of this work follow.

Anode: As stated in Section 6.1.1 and Reference (33), state-of-the-art anodes are made of a Ni-Cr/Ni-Al alloy. The Cr was added to eliminate the problem of anode sintering. However, Ni-Cr anodes are susceptible to creep when placed under the torque load required in the stack to minimize contact resistance between components. The Cr in the anode is also lithiated by the electrolyte; then it consumes carbonate. Developers are trying lesser amounts of Cr (8 percent) to reduce the loss of electrolyte, but some have found that reducing the Cr by 2 percentage points increased creep (34). Several developers have tested Ni-Al alloy anodes that provide creep resistance with minimum electrolyte loss (34, 35, 36). The low creep rate with this alloy is attributed to the formation of $LiAlO_2$ dispersed in Ni (35).

[25]. The area of contact between the outer edge of the bipolar plate and the electrolyte structure prevents gas from leaking out of the anode and cathode compartments. The gas seal is formed by compressing the contact area between the electrolyte structure and the bipolar plate so that the liquid film of molten carbonate at operating temperature does not allow gas to permeate through.

Even though alloys of chromium or aluminum strengthened nickel provides a stable, non-sintering, creep-resistant anode, electrodes made with Ni are relatively high in cost. Alloys, such as Cu-Al and $LiFeO_2$, have not demonstrated sufficient creep strength or performance. Because of this, present research is focused on reducing the manufacturing cost of the nickel alloy anodes (37).

There is a need for better sulfur tolerance in MCFCs, especially when considering coal operation. The potential benefit for sulfur tolerant cells is to eliminate cleanup equipment that impacts system efficiency. This is especially true if low temperature cleanup is required, because the system efficiency and capital cost suffer when the fuel gas temperature is first reduced, then increased to the cell temperature level. Tests are being conducted on ceramic anodes to alleviate the problems, including sulfur poisoning, being experienced with anodes (31). Anodes are being tested with undoped $LiFeO_2$ and $LiFeO_2$ doped with Mn and Nb. Preliminary testing, where several parameters were not strictly controlled, showed that the alternative electrodes exhibited poor performance and would not operate over 80 mA/cm^2. At the present time, no alternative anodes have been identified. Instead, future work will focus on tests to better understand material behavior and to develop alternative materials with emphasis on sulfur tolerance.

Cathode*:* An acceptable material for cathodes must have adequate electrical conductivity, structural strength, and low dissolution rate in molten alkali carbonates to avoid precipitation of metal in the electrolyte structure. State-of-the art cathodes are made of lithiated NiO (33, 38) that have acceptable conductivity and structural strength. However, in early testing, a predecessor of UTC Fuel Cells found that the nickel dissolved, then precipitated and reformed as dendrites across the electrolyte matrix. This decreased performance and eventual short-circuting of the cell. Dissolution of the cathode has turned out to be the primary life-limiting constraint of MCFCs, particularly in pressurized operation (35). Developers are investigating approaches to resolve the NiO dissolution issue. For atmospheric cells, developers are looking at increasing the basicity of the electrolyte (using a more basic melt such as $Li/NaCO_3$). Another approach is to lower CO_2 (acidic) partial pressure. To operate at higher pressures (higher CO_2 partial pressure), developers are investigating alternative materials for the cathodes and using additives in the electrolyte to increase its basicity (37).

Initial work on $LiFeO_2$ cathodes showed that electrodes made with this material were very stable chemically under the cathode environment; there was essentially no dissolution (31). However, these electrodes perform poorly compared to the state-of-the-art NiO cathode at atmospheric pressure because of slow kinetics. The electrode shows promise at pressurized operation, so it is still being investigated. Higher performance improvements are expected with Co-doped $LiFeO_2$. It also has been shown that 5 mol lithium-doped NiO with a thickness of 0.02 cm provided a 43 mV overpotential (higher performance) at 160 mA/cm^2 compared to the state-of-the-art NiO cathode. It is assumed that reconfiguring the structure, such as decreasing the agglomerate size, could improve performance.

Another idea for resolving the cathode dissolution problem is to formulate a milder cell environment. This leads to the approach of using additives in the electrolyte to increase its basicity. Small amounts of additives provide similar voltages to those without additives, but larger amounts adversely affect performance (39). Table 6-2 quantifies the limiting amounts of additives.

Table 6-2 Amount in Mol percent of Additives to Provide Optimum Performance (39)

	62 MOL percent Li_2CO_3/K_2CO_2	52 MOL percent Li_2CO_3/NA_2CO_3
$CaCO_3$	0 to 15	0 to 5
$SrCO_3$	0 to 5	0 to 5
$BaCO_3$	0 to 10	0 to 5

Another approach to a milder cell environment is to increase the fraction of Li in the baseline electrolyte or change the electrolyte to Li/Na rather than the baseline 62/38 Li/K melt (29, 39, 40). Within the past 10 years, a lower cost stabilized cathode was developed with a base material cost comparable to the unstabilized cathode (41). A 100 cm^2 cell test of the lower-cost stabilized cathode with a Li/Na electrolyte system completed 10,000 hours of operation.

Electrolyte Matrix: The present electrolyte structure materials are tightly packed, fine α- or γ-$LiAlO_2$ with fiber or particulate reinforcement. Long-term cell testing reveals significant particle growth and γ to α phase transformation, leading to detrimental changes in the pore structure. The particles grow faster at higher temperatures, in low CO_2 gas atmospheres, and in strongly basic melts. The γ phase is stable at > 700 °C, whereas the α phase is stable at 600 to 650 °C. Such particle growth and phase transformations can be explained by a dissolution - precipitation mechanism. The matrix must also be strong enough to counter operating mechanical and thermal stresses, and still maintain the gas seal. Thermal cycling below the carbonate freezing temperature can induce cracking due to thermo-mechanical stress. Ceramic fiber reinforcement is most effective for crack deflection, followed by platelet and sphere forms. However, strong, cost effective, and stable ceramic fibers are not yet commercially available. Long-term, intense material research may be needed to develop such ceramic fibers. If particle sizes are markedly different, the phase transformation is more controlled by the particle sizes, according to Ostwald ripening where small particles preferentially dissolve and re-precipitate onto larger particles. Therefore, a more uniform particle size distribution is needed to maintain a desired pore structure. The industry trend is to switch from γ-$LiAlO_2$ to α-$LiAlO_2$ for better long-term phase and particle-size stabilities. FCE is developing a low-cost $LiAlO_2$, aqueous-base manufacturing system, but must resolve slow drying rate of $LiAlO_2$ and its instability in water (42).

Electrolyte: Present electrolytes have the following chemistry: lithium potassium carbonate, Li_2CO_3/K_2CO_3 (62:38 mol percent) for atmospheric pressure operation and lithium sodium carbonate, $LiCO_3/NaCO_3$ (52:48 o 60:40 mol percent) that is better for improved cathode stability under pressurized operation and life extension. The electrolyte composition affects electrochemical activity, corrosion, and electrolyte loss rate. Evaporation of the electrolyte is a life-limiting issue for the molten carbonate fuel cell. Li/Na electrolyte is better for higher-pressure operation than Li/K because it gives higher performance. This allows the electrolyte matrix to be made thicker for the same performance relative to the Li/K electrolyte. Thicker electrolytes result in a longer time to shorting by internal precipitation. Li/Na also provides

better corrosion resistance to mitigate acidic cathode dissolution. However, it has lower wettability and greater temperature sensitivity. Additives are being investigated to minimize the temperature sensitivity of Li/Na. The electrolyte has a low vapor pressure at operating temperature, and may slowly evaporate. Stack testing has shown that the electrolyte vapor loss is significantly slower than expected. The evaporation loss is projected to have minimal impact on stack life.

***Electrolyte Structure**:* Ohmic losses contribute about a 65 mV loss at the beginning of life, and may increase to as much as 145 mV by 40,000 hours (16). The majority of the voltage loss is in the electrolyte and the cathode components. The electrolyte offers the highest potential for reduction because 70 percent of the total cell ohmic loss occurs there. FCE investigated increasing the porosity of the electrolyte 5 percent to reduce the matrix resistance by 15 percent, and change the melt to Li/Na from Li/K to reduce the matrix resistivity by 40 percent. Work is continuing on the interaction of the electrolyte with the cathode components. At the present time, an electrolyte loss of 25 percent of the initial inventory can be projected with a low surface area cathode current collector and with the proper selection of material.

Another area for electrolyte improvement is the ability to prevent gas crossover from one electrode to the other. FCE produced an improved matrix fabrication process providing low temperature binder burnout. FCE reported in 1997 that it had developed a high performance rugged matrix that increases the gas sealing efficiency by approximately a factor of ten better than the design goal (43).

***Electrolyte Migration**:* There is a tendency for the electrolyte to migrate from the positive end of the stack to the negative end of the stack. This may cause the end cells to lose performance compared to the central cells. The electrolyte loss is through the gasket used to couple the external manifolds to the cell stack. The standard gasket material is porous and provides a conduit for electrolyte transfer. A new gasket design incorporating electrolyte flow barriers inside the gasket (US Patent 5,110,692) plus end cell inventory capability offers the potential for reaching 40,000 hours, if only this mode of failure is considered. Stacks with internal manifolding do not require a gasket, and may not experience this problem (44).

Bipolar Plate: The present bipolar plate consists of a separator, current collectors, and the wet seal. The separator and current collector is Ni-coated 310S/316L and the wet seal is formed by aluminization of the metal. The plate is exposed to the anode environment of one side and the cathode environment on the other. Low oxygen partial pressure on the anode side of the bipolar plate prevents the formation of a protective oxide coating. After reaction with the thin, creeping electrolyte, heat-resistant alloys form a multi-layered corrosion scale. This condition may be accelerated by carbonization, higher temperature, and higher moisture gas environment. On the cathode side, contact electrical resistance increases as an oxide scale builds up. Electrolyte loss due to corrosion and electrolyte creep also contributes to power decay. Single alloy bipolar current collector materials that function well in both anode and cathode environments need to be developed. Although such development has been attempted, high cost and high ohmic resistance prevent it from being successful. Presently, stainless steels, particularly austenitic stainless steels, are the primary construction materials. More expensive nickel-based alloys resist corrosion as well as or only slightly better than austenitic stainless steels. A thermodynamically

stable nickel coating is needed to protect the anode side. Unfortunately, electroless nickel coatings, although dense or uniform in thickness, are expensive and contain detrimental impurities; electrolytic nickel coatings are not sufficiently dense or uniform in thickness. FCE and others have found that cladding with nickel provides excellent corrosion protection. A nickel cladding of 50 μm thickness is projected for >40,000 hours of life (42).

Coal Gas Trace Species: MCFCs to date have been operated on reformed or simulated natural gas and simulated coal gas. Testing conducted with simulated coal gas has involved the expected individual and multi-trace constituents to better understand coal operation (45).

Table 6-3 shows the contaminants and their impact on MCFC operation. The table denotes the species of concern and what cleanup of the fuel gas is required to operate on coal gas. Confidence in operation with coal will require the use of an actual gasifier product. An FCE MCFC stack was installed (fall of 1993) using a slipstream of an actual coal gasifier to further clarify the issues of operation with trace gases (46).

Table 6-3 Qualitative Tolerance Levels for Individual Contaminants in Isothermal Bench-Scale Carbonate Fuel Cells (46, 47, and 48)

CONTAMINANTS (typical ppm in raw coal gas)	REACTION MECHANISM	QUALITATIVE TOLERANCES	CONCLUSIONS
NO NOTICEABLE EFFECTS			
NH_3 (10,000) Cd (5) Hg (1) Sn (3)	$2NH_3 \rightarrow N_2+3H_2$ $Cd+H_2O \rightarrow CdO(s)+H_2$ (Hg Vapor Not Reactive) (Sn(l) Not Volatile)	~1 vol percent NH_3 ~30 ppm Cd 35 ppm Hg No Vapor @ 650°C	No Effects No Cell Deposits No TGA Effects No Cell Deposits
MINOR EFFECTS			
Zn (100) Pb (15)	$Zn+H_2O \rightarrow ZnO(s)+H_2$ $Pb+H_2O \rightarrow PbS(s)+H_2$	<15 ppm Zn 1.0 ppm Pb sat'd vapor	No Cell Deposits at 75 percent Utilization Cell Deposits Possible in Presence of High H_2Se
SIGNIFICANT EFFECTS			
H_2S (15,000) HCl (500) H_2Se (5) As (10)	$xH_2S+Ni \rightarrow NiS_x+xH_2$ $2HCl+K_2CO_3 \rightarrow 2KCl(v)+H_2O/CO_2$ $xH_2Se+Ni \rightarrow NiSe_x+xH_2$ $AsH_3+Ni \rightarrow NiAs(s)+3/2H_2$	<0.5 ppm H_2S <0.1 ppm HCl <0.2 ppm H_2Se <0.1 ppm As	Recoverable Effect Long Term Effects Possible Recoverable Effect Cumulative Long Term Effect

6.2 Performance

Factors affecting the selection of operating conditions are stack size, heat transfer rate, voltage level, load requirement, and cost. The performance curve is defined by cell pressure, temperature, gas composition, and utilization. Typical MCFCs will generally operate in the range of 100 to 200 mA/cm^2 at 750 to 900 mV/cell.

Typical cathode performance curves obtained at 650 °C with an oxidant composition (12.6 percent O_2/18.4 percent CO_2/69 percent N_2) that is anticipated for use in MCFCs, and a common baseline composition (33 percent O_2/67 percent CO_2) are presented in Figure 6-4 (22, 49). The baseline

composition contains O_2 and CO_2 in the stoichiometric ratio that is needed in the electrochemical reaction at the cathode (Equation (6-2)). With this gas composition, little or no diffusion limitations occur in the cathode because the reactants are provided primarily by bulk flow. The other gas composition, which contains a substantial fraction of N_2, yields a cathode performance that is limited dilution by an inert gas.

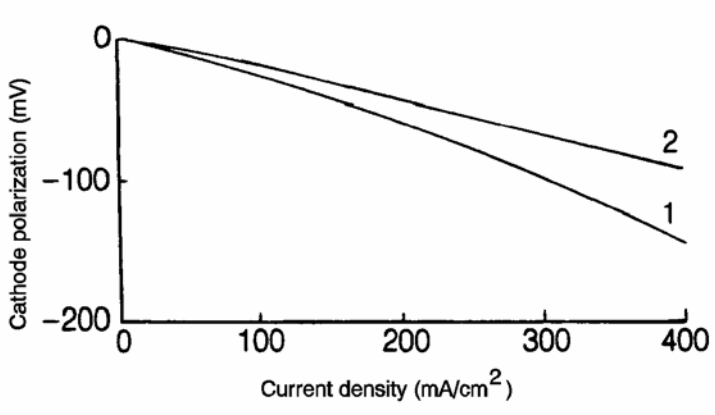

Figure 6-4 Effect of Oxidant Gas Composition on MCFC Cathode Performance at 650°C, (Curve 1, 12.6 percent O_2/18.4 percent CO_2/69.0 percent N_2; Curve 2, 33 percent O_2/67 percent CO_2)

In the 1980s, the performance of MCFC stacks increased dramatically. During the 1990s, cells as large as 1.0 m^2 are being tested in stacks. Most recently, the focus has been on achieving performance in a stack equivalent to single cell performance. Cells with an electrode area of 0.3 m^2 were routinely tested at ambient and above ambient pressures with improved electrolyte structures made by tape-casting processes (22). Several stacks underwent endurance testing in the range of 7,000 to 10,000 hours. The voltage and power as a function of current density after 960 hours for a 1.0 m^2 stack consisting of 19 cells are shown in Figure 6-5. The data were obtained with the cell stack at 650 °C and 1 atmosphere.

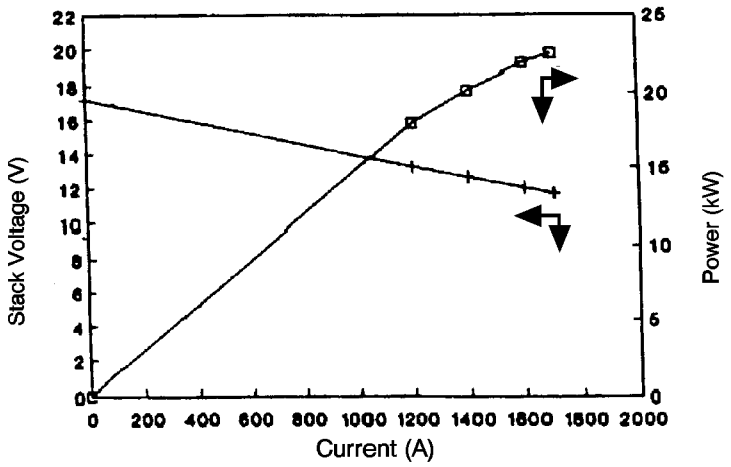

Figure 6-5 Voltage and Power Output of a 1.0/m^2 19 cell MCFC Stack after 960 Hours at 965 °C and 1 atm, Fuel Utilization, 75 percent (50)

The remainder of this section will review operating parameters that affect MCFC performance. Supporting data will be presented, as well as equations derived from empirical analysis.

6.2.1 Effect of Pressure

The dependence of reversible cell potential on pressure is evident from the Nernst equation. For a change in pressure from P_1 to P_2, the change in reversible potential (ΔV_p) is given by

$$\Delta V_p = \frac{RT}{2F} \ln \frac{P_{1,a}}{P_{2,a}} + \frac{RT}{2F} \ln \frac{P_{2,c}^{3/2}}{P_{1,c}^{3/2}} \qquad (6\text{-}11)$$

where the subscripts a and c refer to the anode and cathode, respectively. In an MCFC with the anode and cathode compartments at the same pressure (i.e., $P_1=P_{1,a}=P_{1,c}$ and $P_2=P_{2,a}=P_{2,c}$):

$$\Delta V_p = \frac{RT}{2F} \ln \frac{P_1}{P_2} + \frac{RT}{2F} \ln \frac{P_2^{3/2}}{P_1^{3/2}} = \frac{RT}{4F} \ln \frac{P_2}{P_1} \qquad (6\text{-}12)$$

At 650 °C

$$\Delta V_p \text{ (mV)} = 20 \ln \frac{P_2}{P_1} = \left(46 \log \frac{P_2}{P_1} \right) \qquad (6\text{-}13)$$

Thus, a tenfold increase in cell pressure corresponds to an increase of 46 mV in the reversible cell potential at 650 °C.

Increasing the operating pressure of MCFCs results in enhanced cell voltages because of the increase in the partial pressure of the reactants, increase in gas solubilities, and increase in mass transport rates. Opposing the benefits of increased pressure are the effects of pressure on undesirable side reactions such as carbon deposition (Boudouard reaction):

$$2CO \rightarrow C + CO_2 \qquad (6\text{-}14)$$

and methane formation (methanation)

$$CO + 3H_2 \rightarrow CH_4 + H_2O \qquad (6\text{-}15)$$

In addition, decomposition of CH_4 to carbon and H_2 is possible

$$CH_4 \rightarrow C + 2H_2 \qquad (6\text{-}16)$$

but this reaction is suppressed at higher pressure. According to Le Chatelier's principle, an increase in pressure will favor carbon deposition by Equation (6-14)[26] and methane formation by Equations (6-15) and (6-16) (51). The water-gas shift reaction (52)[27]

$$CO_2 + H_2 \leftrightarrow CO + H_2O \qquad (6\text{-}17)$$

is not affected by an increase in pressure because the number of moles of gaseous reactants and products in the reaction is identical. Carbon deposition in an MCFC is to be avoided because it can lead to plugging of the gas passages in the anode. Methane formation is detrimental to cell performance because the formation of each mole consumes three moles of H_2, which represents a considerable loss of reactant and would reduce power plant efficiency.

The addition of H_2O and CO_2 to the fuel gas modifies the equilibrium gas composition so that the formation of CH_4 is not favored. Increasing the partial pressure of H_2O in the gas stream can

[26]. Data from translation of Russian literature (51) indicate the equilibrium constant is almost independent of pressure.

[27]. Data from translation of Russian literature (52) indicate the equilibrium constant K is a function of pressure. In relative terms, if K (627 °C) = 1 at 1 atm, it decreases to 0.74K at 500 atm and 0.60K at 1000 atmospheres. At the operating pressures of the MCFC, the equilibrium constant can be considered invariant with pressure.

reduce carbon deposition. Measurements (22) on 10 cm x 10 cm cells at 650 °C using simulated gasified coal GF-1 (38 percent H_2/56 percent CO/6 percent CO_2) at 10 atm showed that only a small amount of CH_4 is formed. At open circuit, 1.4 vol percent CH_4 (dry gas basis) was detected, and at fuel utilizations of 50 to 85 percent, 1.2 to 0.5 percent CH_4 was measured. The experiments with a high CO fuel gas (GF-1) at 10 atmospheres and humidified at 163 °C showed no indication of carbon deposition in a subscale MCFC. These studies indicated that CH_4 formation and carbon deposition at the anodes in an MCFC operating on coal-derived fuels can be controlled, and under these conditions, the side reactions would have little influence on power plant efficiency.

Figure 6-6 shows the effect of pressure (3, 5, and 10 atmospheres) and oxidant composition (3.2 percent CO_2/23.2 percent O_2/66.3 percent N_2/7.3 percent H_2O and 18.2 percent CO_2/9.2 percent O_2/65.3 percent N_2/7.3 percent H_2O) on the performance of 70.5 cm^2 MCFCs at 650 °C (53). The major difference as the CO_2 pressure changes is the change in open circuit potential, which increases with cell pressure and CO_2 content (see Equation (6-11)). At 160 mA/cm^2, ΔV_p is -44 mV for a pressure change from 3 to 10 atmospheres for both oxidant compositions.

Because ΔV_p is a function of the total gas pressure, the gas compositions in Figure 6-6 have little influence on ΔV_p. Based on these results, the effect of cell voltage from a change in pressure can be expressed by the equation

$$\Delta V_p \text{ (mV)} = 84 \log \frac{P_2}{P_1} \qquad \textit{(6-18)}$$

where P_1 and P_2 are different cell pressures. Another analysis by Benjamin, et al. (54) suggests that a coefficient less than 84 may be more applicable. The change in voltage as a function of pressure change was expressed as

$$\Delta V_p \text{ (mV)} = 76.5 \log \frac{P_2}{P_1} \qquad \textit{(6-19)}$$

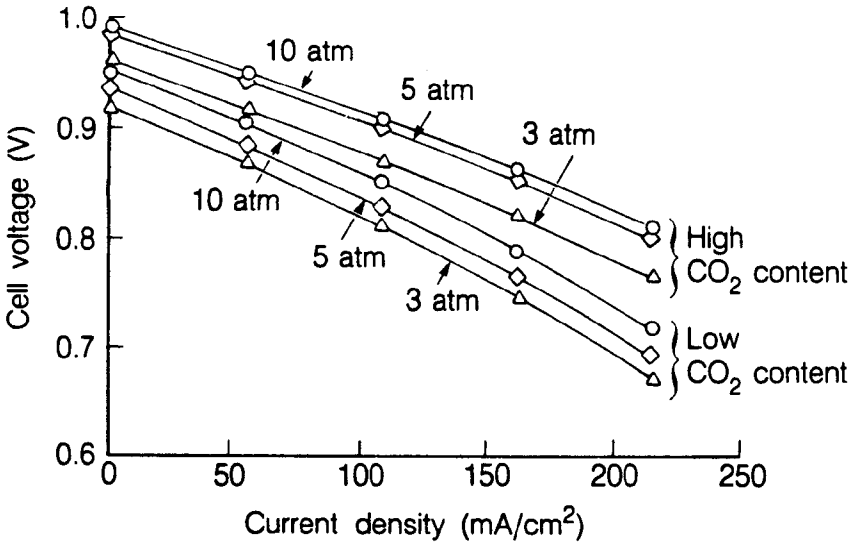

Figure 6-6 Influence of Cell Pressure on the Performance of a 70.5 cm^2 MCFC at 650 °C (anode gas, not specified; cathode gases, 23.2 percent O_2/3.2 percent CO_2/66.3 percent N_2/7.3 percent H_2O and 9.2 percent O_2/18.2 percent CO_2/65.3 percent N_2/7.3 percent H_2O; 50 percent CO_2, utilization at 215 mA/cm^2) (53, Figure 4, Pg. 395)

Equation (6-19) was based on a load of 160 mA/cm^2 at a temperature of 650 °C. It was also found to be valid for a wide range of fuels and for a pressure range of 1 atmosphere $\leq P \leq$ 10 atmospheres. Other results (55) support this coefficient. Figure 6-7 shows the influence of pressure change on voltage gain for three different stack sizes. These values are for a temperature of 650 °C and a constant current density of 150 mA/cm^2 at a fuel utilization of 70 percent. The line that corresponds to a coefficient of 76.5 falls approximately in the middle of these values. Further improvements in cell performance will lead to changes in the logarithmic coefficient. Additional data (56, 57, 58) indicate that the coefficient may indeed be less than 76.5, but Equation (6-19) appears to represent the effect of pressure change on performance.

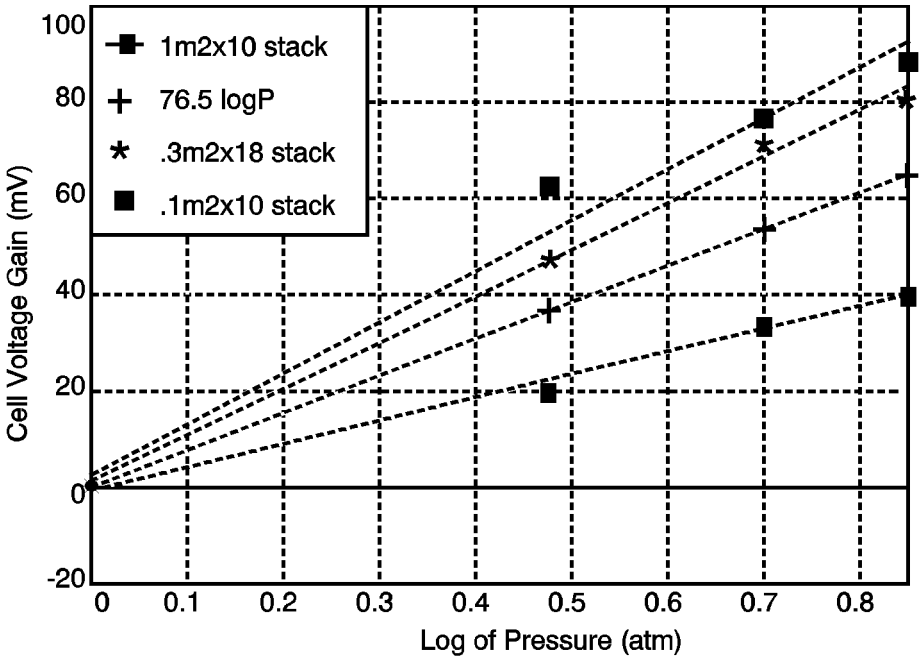

Figure 6-7 Influence of Pressure on Voltage Gain (55)

6.2.2 Effect of Temperature

The influence of temperature on the reversible potential of MCFCs depends on several factors, one of which involves the equilibrium composition of the fuel gas (22, 59, 60, 61).[28] The water gas shift reaction achieves rapid equilibrium[29] at the anode in MCFCs, and consequently CO serves as an indirect source of H_2. The equilibrium constant (K)

$$K = \frac{P_{CO} P_{H_2O}}{P_{H_2} P_{CO_2}} \qquad (6\text{-}20)$$

increases with temperature (see Table 6-4 and Appendix 10.1), and the equilibrium composition changes with temperature and utilization to affect the cell voltage.

The influence of temperature on the voltage of MCFCs is illustrated by the following example. Consider a cell with an oxidant gas mixture of 30 percent O_2/60 percent CO_2/10 percent N_2, and a fuel gas mixture of 80 percent H_2/20 percent CO_2. When the fuel gas is saturated with H_2O vapor at 25 °C, its composition becomes 77.5 percent H_2/19.4 percent CO_2/3.1 percent H_2O.

---

[28]. For a fixed gas composition of H_2, H_2O, CO, CO_2, and CH_4 there is a temperature, T_b, below which the exothermic Boudouard reaction is thermodynamically favored, and a temperature, T_m, above which carbon formation by the endothermic decomposition of CH_4 is thermodynamically favored; more extensive details on carbon deposition are found elsewhere (22, 59, 60, 61).

[29]. The dependence of equilibrium constant on temperature for carbon deposition, methanation, and water gas shift reactions is presented in Appendix 10.1.

After considering the equilibrium established by the water gas shift reaction, the equilibrium concentrations can be calculated (see Example 9-5 in Section 9) using Equation (6-20) and the equilibrium constant; see for instance, Broers and Treijtel (62). The equilibrium concentrations are substituted into Equation (6-4) to determine E as a function of T.

Table 6-4 Equilibrium Composition of Fuel Gas and Reversible Cell Potential as a Function of Temperature

Parameter[a]	Temperature (°K)		
	800	900	1000
P_{H_2}	0.669	0.649	0.643
P_{CO_2}	0.088	0.068	0.053
P_{CO}	0.106	0.126	0.141
P_{H_2O}	0.137	0.157	0.172
E[b] (V)	1.155	1.143	1.133
K[c]	0.2474	0.4538	0.7273

a - P is the partial pressure computed from the water gas shift equilibrium of inlet gas with composition77.5 percent H_2/19.4 percent CO_2/3.1 percent H_2O at 1 atmosphere.
b - Cell potential calculated using Nernst equation and cathode gas composition of 30 percent O_2/60 percent CO_2/10 percent N_2.
c - Equilibrium constant for water gas shift reaction from Reference (59).

The results of these calculations are presented in Table 6-4. Inspection of the results shows a change in the equilibrium gas composition with temperature. The partial pressures of CO and H_2O increase at higher T because of the dependence of K on T. The result of the change in gas composition, and the decrease in E° with increasing T, is that E decreases with an increase in T. In an operating cell, the polarization is lower at higher temperatures, and the net result is that a higher cell voltage is obtained at elevated temperatures. The electrode potential measurements (9) in a 3 cm^2 cell[30] show that the polarization at the cathode is greater than at the anode, and that the polarization is reduced more significantly at the cathode with an increase in temperature. At a current density of 160 mA/cm^2, cathode polarization is reduced by about 160 mV when the temperature increases from 550 to 650 °C, whereas the corresponding reduction in anode polarization is only about 9 mV (between 600 and 650 °C, no significant difference in polarization is observed at the anode).

Baker, et al. (63) investigated the effect of temperature (575 to 650 °C) on the initial performance of small cells (8.5 cm^2). With steam-reformed natural gas as the fuel and 30 percent

[30]. Electrolyte is 55 wt% carbonate eutectic (57 wt% Li_2CO_3, 31 wt% Na_2CO_3, 12 wt% K_2CO_3) and 45 wt% $LiA1O_2$, anode is Co + 10% Cr, cathode is NiO, fuel is 80% H_2/20% CO_2 and oxidant is 30% CO_2/70% air.

CO_2/70 percent air as the oxidant, the cell voltage[31] at 200 mA/cm^2 decreased by 1.4 mV/° for a reduction in temperature from 650 to 600 °C, and 2.16 mV/°C for a decrease from 600 to 575 °C. In the temperature range 650 to 700 °C, data analysis (58) indicates a relationship of 0.25 mV/° C. The following equations summarize these results.

$$\Delta V_T \text{ (mV)} = 2.16\ (T_2 - T_1) \qquad 575°C \leq T < 600\ °C \qquad \textit{(6-21)}$$

$$\Delta V_T \text{ (mV)} = 1.40\ (T_2 - T_1) \qquad 600°C \leq T < 650\ °C \qquad \textit{(6-22)}$$

$$\Delta V_T \text{ (mV)} = 0.25\ (T_2 - T_1) \qquad 650°C < T \leq 700\ °C \qquad \textit{(6-23)}$$

The two major contributors responsible for the change in cell voltage with temperature are the ohmic polarization and electrode polarization. It appears that in the temperature range of 575 to 650 °C, about 1/3 of the total change in cell voltage with decreasing temperature is due to an increase in ohmic polarization, and the remainder from electrode polarization at the anode and cathode. Most MCFC stacks currently operate at an average temperature of 650 °C. Most carbonates do not remain molten below 520 °C, and as seen by the previous equations, increasing temperature enhances cell performance. Beyond 650 °C, however, there are diminishing gains with increased temperature. In addition, there is increased electrolyte loss from evaporation and increased material corrosion. An operating temperature of 650 °C thus offers a compromise between high performance and stack life.

6.2.3 Effect of Reactant Gas Composition and Utilization

The voltage of MCFCs varies with the composition of the reactant gases. The effect of reactant gas partial pressure, however, is somewhat difficult to analyze. One reason involves the water gas shift reaction at the anode due to the presence of CO. The other reason is related to the consumption of both CO_2 and O_2 at the cathode. Data (55, 64, 65, 66) show that increasing the reactant gas utilization generally decreases cell performance.

As reactant gases are consumed in an operating cell, the cell voltage decreases in response to the polarization (i.e., activation, concentration) and to the changing gas composition. These effects are related to the partial pressures of the reactant gases.

Oxidant: The electrochemical reaction at the cathode involves the consumption of two moles CO_2 per mole O_2 (see Equation (6-2)), and this ratio provides the optimum cathode performance. The influence of the $[CO_2]/[O_2]$ ratio on cathode performance is illustrated in Figure 6-8 (22). As this ratio decreases, the cathode performance decreases, and a limiting current is discernible. In the

[31]. Cell was operated at constant flow rate; thus, the utilization changes with current density.

limit where no CO_2 is present in the oxidant feed, the equilibrium involving the dissociation of carbonate ions becomes important.

$$CO_3^{=} \leftrightarrow CO_2 + O^{=} \qquad (6\text{-}24)$$

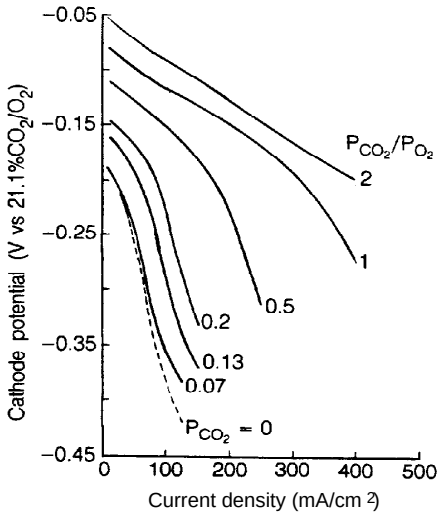

Figure 6-8 Effect of CO_2/O_2 Ratio on Cathode Performance in an MCFC, Oxygen Pressure is 0.15 atm (22, Figure 5-10, Pgs. 5-20)

Under these conditions, the cathode performance shows the greatest polarization because of the composition changes that occur in the electrolyte. The change in the average cell voltage of a ten-cell stack as a function of oxidant utilization is illustrated in Figure 6-9. In this stack, the average cell voltage at 172 mA/cm^2 decreases by about 30 mV for a 30 percentage point increase in oxidant (20 to 50 percent) utilization. Based on this additional data (55, 64, 65), the voltage loss due to a change in oxidant utilization can be described by the following equations:

$$\Delta V_{cathode}\,(mV) = 250 \log \frac{\left(\overline{P}_{CO_2}\ \overline{P}_{O_2}^{\frac{1}{2}}\right)_2}{\left(\overline{P}_{CO_2}\ \overline{P}_{O_2}^{\frac{1}{2}}\right)_1} \qquad \text{for } 0.04 \le \left(\overline{P}_{CO_2}\ \overline{P}_{O_2}^{\frac{1}{2}}\right) \le 0.11 \qquad (6\text{-}25)$$

$$V_{cathode}\,(mV) = 99 \log \frac{\left(\overline{P}_{CO_2}\ \overline{P}_{O_2}^{\frac{1}{2}}\right)_2}{\left(\overline{P}_{CO_2}\ \overline{P}_{O_2}^{\frac{1}{2}}\right)_1} \qquad \text{for } 0.11 < \left(\overline{P}_{CO_2}\ \overline{P}_{O_2}^{\frac{1}{2}}\right) \le 0.38 \qquad (6\text{-}26)$$

where $\overline{P}_{CO_2}$ and $\overline{P}_{O_2}$ are the average partial pressures of CO_2 and O_2 in the system.

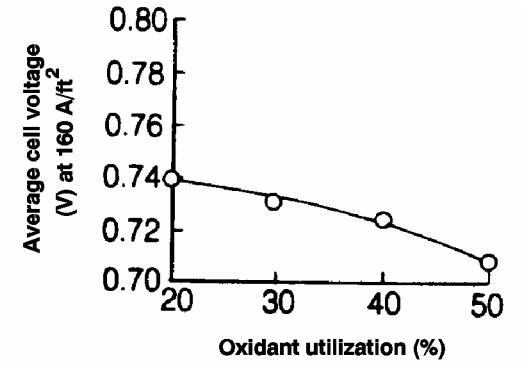

Figure 6-9 Influence of Reactant Gas Utilization on the Average Cell Voltage of an MCFC Stack (67, Figure 4-21, Pgs. 4-24)

Fuel: The data in Table 6-5 from Lu and Selman (68) illustrate the dependence of the anode potential on the composition of five typical fuel gases and two chemical equilibria occurring in the anode compartment.[32] The calculations show the gas compositions and open circuit anode potentials obtained after equilibria by the water gas shift and CH_4 steam reforming reactions are considered. The open circuit anode potential calculated for the gas compositions after equilibration, and experimentally measured, is presented in Table 6-5. The equilibrium gas compositions obtained by the shift and steam reforming reactions clearly show that, in general, the H_2 and CO_2 contents in the dry gas decrease, and CH_4 and CO are present in the equilibrated gases. The anode potential varies as a function of the $[H_2]/[H_2O][CO_2]$ ratio; a higher potential is obtained when this ratio is higher. The results show that the measured potentials agree with the values calculated, assuming that simultaneous equilibria of the shift and the steam reforming reactions reach equilibrium rapidly in the anode compartments of MCFCs.

[32]. No gas phase equilibrium exists between O_2 and CO_2 in the oxidant gas that could alter the composition or cathode potential.

Table 6-5 Influence of Fuel Gas Composition on Reversible Anode Potential at 650 °C (68, Table 1, Pg. 385)

Typical Fuel Gas[a]	Gas Composition (mole fraction) H_2	H_2O	CO	CO_2	CH_4	N_2	-E[b] (mV)
Dry gas							
High Btu (53 °C)	0.80	-	-	0.20	-	-	1116±3[c]
Intermed. Btu (71 °C)	0.74	-	-	0.26	-	-	1071±2[c]
Low Btu 1 (71 °C)	0.213	-	0.193	0.104	0.011	0.479	1062±3[c]
Low Btu 2 (60 °C)	0.402	-	-	0.399	-	0.199	1030±[c]
Very low Btu (60 °C)	0.202	-	-	0.196	-	0.602	1040±[c]
Shift equilibrium							
High Btu (53 °C)	0.591	0.237	0.096	0.076	-	-	1122[d]
Intermed. Btu (71 °C)	0.439	0.385	0.065	0.112	-	-	1075[d]
Low Btu 1 (71 °C)	0.215	0.250	0.062	0.141	0.008	0.326	1054[d]
Low Btu 2 (60 °C)	0.231	0.288	0.093	0.228	-	0.160	1032[d]
Very low Btu (60 °C)	0.128	0.230	0.035	0.123	-	0.484	1042[d]
Shift and Steam-reforming							
High Btu (53 °C)	0.555	0.267	0.082	0.077	0.020	-	1113[d]
Intermed. Btu (71 °C)	0.428	0.394	0.062	0.112	0.005	-	1073[d]
Low Btu 1 (71 °C)	0.230	0.241	0.067	0.138	0.001	0.322	1059[d]
Low Btu 2 (60 °C)	0.227	0.290	0.092	0.229	0.001	0.161	1031[d]
Very low Btu (60 °C)	0.127	0.230	0.035	0.123	0.0001	0.485	1042[d]

a - Temperature in parentheses is the humidification temperature
b - Anode potential with respect to 33 percent O_2/67 percent CO_2 reference electrode
c - Measured anode potential
d - Calculated anode potential, taking into account the equilibrated gas composition

Further considering the Nernst equation, an analysis shows that the maximum cell potential for a given fuel gas composition is obtained when $[CO_2]/[O_2] = 2$. Furthermore, the addition of inert gases to the cathode, for a given $[CO_2]/[O_2]$ ratio, causes a decrease in the reversible potential. On the other hand, the addition of inert gases to the anode increases the reversible potential for a given $[H_2]/[H_2O][CO_2]$ ratio and oxidant composition. This latter result occurs because two moles of product are diluted for every mole of H_2 reactant. However, the addition of inert gases to either gas stream in an operating cell can lead to an increase in concentration polarization.

Figure 6-10 depicts an average voltage loss for the stack of about 30 mV for a 30 percent increase in fuel utilization (30 to 60 percent). This and other data (66) suggest that the voltage loss due to a change in fuel utilization can be described by the following equation:

$$\Delta V_{anode}\,(mV) = 173 \log \frac{\left(\overline{P}_{H_2} / \overline{P}_{CO_2}\,\overline{P}_{H_2O}\right)_2}{\left(\overline{P}_{H_2} / \overline{P}_{CO_2}\,\overline{P}_{H_2O}\right)_1} \qquad (6\text{-}27)$$

where $\overline{P}_{H_2}$, $\overline{P}_{CO_2}$, and $\overline{P}_{H_2O}$ are the average partial pressures of H_2, CO_2, and O_2 in the system.

The above discussion implies that MCFCs should be operated at low reactant gas utilizations to maintain voltage levels, but doing this means inefficient fuel use. As with other fuel cell types, a compromise must be made to optimize overall performance. Typical utilizations are 75 to 85 percent of the fuel.

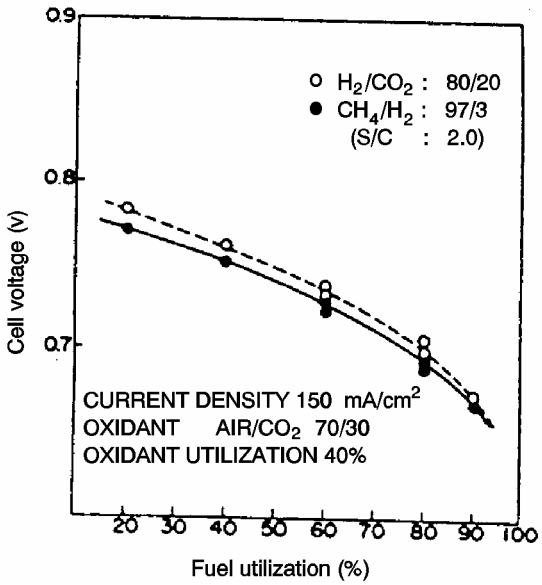

Figure 6-10 Dependence of Cell Voltage on Fuel Utilization (69)

6.2.4 Effect of Impurities

Gasified coal is expected to be the major source of fuel gas for MCFCs, but because coal contains many contaminants in a wide range of concentrations, fuel derived from this source also contains a considerable number of contaminants.[33] A critical concern with these contaminants is the concentration levels that can be tolerated by MCFCs without significant degradation in

[33]. See Table 11.1 for contaminant levels found in fuel gases from various coal gasification processes.

performance or reduction in cell life. A list of possible effects of contaminants from coal-derived fuel gases on MCFCs is summarized in Table 6-6 (70).

Table 6-6 Contaminants from Coal-Derived Fuel Gas and Their Potential Effect on MCFCs (70, Table 1, Pg. 299)

Class	Contaminant	Potential Effect
Particulates	Coal fines, ash	• Plugging of gas passages
Sulfur compounds	H_2S, COS, CS_2, C_4H_4S	• Voltage losses • Reaction with electrolyte via SO_2
Halides	HCl, HF, HBr, $SnCl_2$	• Corrosion • Reaction with electrolyte
Nitrogen compounds	NH_3, HCN, N_2	• Reaction with electrolyte via NO_X
Trace metals	As, Pb, Hg, Cd, Sn Zn, H_2Se, H_2Te, AsH_3	• Deposits on electrode • Reaction with electrolyte
Hydrocarbons	C_6H_6, $C_{10}H_8$, $C_{14}H_{10}$	• Carbon deposition

The typical fuel gas composition and contaminants from an air-blown gasifier that enter the MCFC at 650 °C after hot gas cleanup, and the tolerance level of MCFCs to these contaminants are listed in Table 6-7 (79, 71, 72). It is apparent from this example that a wide spectrum of contaminants is present in coal-derived fuel gas. The removal of these contaminants can add considerably to the efficiency. A review of various options for gas cleanup is presented by Anderson and Garrigan (70) and Jalan, et al. (73).

Sulfur*:* It is well established that sulfur compounds in low parts per million concentrations in fuel gas are detrimental to MCFCs (74, 75, 76, 77, 78). The tolerance of MCFCs to sulfur compounds (74) is strongly dependent on temperature, pressure, gas composition, cell components, and system operation (i.e., recycle, venting, gas cleanup). The principal sulfur compound that has an adverse effect on cell performance is H_2S. At atmospheric pressure and high gas utilization (~75 percent), <10 ppm H_2S in the fuel can be tolerated at the anode (tolerance level depends on anode gas composition and partial pressure of H_2), and <1 ppm SO_2 is acceptable in the oxidant (74). These concentration limits increase when the temperature increases, but they decrease at increasing pressures.

Table 6-7 Gas Composition and Contaminants from Air-Blown Coal Gasifier After Hot Gas Cleanup, and Tolerance Limit of MCFCs to Contaminants

Fuel Gas[a] (mol percent)	Contaminants[b,c]	Content[b,c]	Remarks[b]	Tolerance[c,d] Limit
19.2 CO	Particulates	<0.5 mg/l	Also includes ZnO from H_2S cleanup stage	<0.1 g/l for large particulates >0.3 :m
13.3 H_2	NH_3	2600 ppm		<10,000 ppm
2.6 CH_4	AsH_3	<5 ppm		< 1 ppm
6.1 CO_2	H_2S	<10 ppm	After first-stage cleanup	<0.5 ppm
12.9 H_2O	HCl	500 ppm	Also includes other halides	<10 ppm
45.8 N_2	Trace Metals	<2 ppm <2 ppm <2 ppm <2 ppm	Pb Cd Hg Sn	<1 ppm 30+ ppm 35+ ppm NA
	Zn	<50 ppm	From H_2S hot cleanup	<20 ppm
	Tar	4000 ppm	Formed during desulfurization cleanup stage	<2000 ppm[e]

a - Humidified fuel gas enters MCFC at 650 °C
b - (71, Table 1, Pg. 177)
c - (79)
d - (72)
e - Benzene

The mechanisms by which H_2S affects cell performance have been investigated extensively (75, 76, 77, 78). The adverse effects of H_2S occur because of:

- Chemisorption on Ni surfaces to block active electrochemical sites,
- Poisoning of catalytic reaction sites for the water gas shift reaction, and
- Oxidation to SO_2 in a combustion reaction, and subsequent reaction with carbonate ions in the electrolyte.

The adverse effect of H_2S on the performance of MCFCs is illustrated in Figure 6-11. The cell voltage of a 10 cm x 10 cm cell at 650 °C decreases when 5 ppm H_2S is added to the fuel gas (10 percent H_2/5 percent CO_2/10 percent H_2O/75 percent He), and current is drawn from the cell. The measurements indicate that low concentrations of H_2S do not affect the open circuit potential, but they have a major impact on the cell voltage as current density is progressively increased. The decrease in cell voltage is not permanent;[34] when fuel gas without H_2S is introduced into the cell, the cell voltage returns to the level for a cell with clean fuel. These results can be explained by the chemical and electrochemical reactions that occur involving H_2S and $S^{=}$. A nickel anode at anodic potentials reacts with H_2S to form nickel sulfide:

$$H_2S + CO_3^{=} \rightarrow H_2O + CO_2 + S^{=} \qquad (6\text{-}28)$$

followed by

$$Ni + xS^{=} \rightarrow NiS_x + 2xe^{-} \qquad (6\text{-}29)$$

When the sulfided anode returns to open circuit, the NiS_x is reduced by H_2:

$$NiS_x + xH_2 \rightarrow Ni + xH_2S \qquad (6\text{-}30)$$

Similarly, when a fuel gas without H_2S is introduced to a sulfided anode, reduction of NiS_x to Ni can also occur. Detailed discussions on the effect of H_2S on cell performance are presented by Vogel and co-workers (75, 76) and Remick (77, 78).

The rapid equilibration of the water gas shift reaction in the anode compartment provides an indirect source of H_2 by the reaction of CO and H_2O. If H_2S poisons the active sites for the shift reaction, this equilibrium might not be established in the cell, and a lower H_2 content than predicted would be expected. Fortunately, evidence (77, 78) indicates that the shift reaction is not significantly poisoned by H_2S. In fact, Cr used in stabilized-Ni anodes appears to act as a sulfur tolerant catalyst for the water gas shift reaction (78).

The CO_2 required for the cathode reaction is expected to be supplied by recycling the anode gas exhaust (after combustion of the residual H_2) to the cathode. Therefore, any sulfur in the anode effluent will be present at the cathode inlet unless provisions are made for sulfur removal. In the absence of sulfur removal, sulfur enters the cathode inlet as SO_2, which reacts quantitatively (equilibrium constant is 10^{15} to 10^{17}) with carbonate ions to produce alkali sulfates. These sulfate

[34]. The effects of H_2S on cell voltage are reversible if H_2S concentrations are present at levels below that required to form nickel sulfide.

ions are transported through the electrolyte structure to the anode during cell operation. At the anode, $SO_4^{=}$ is reduced to $S^{=}$, thus increasing the concentration of $S^{=}$ there.

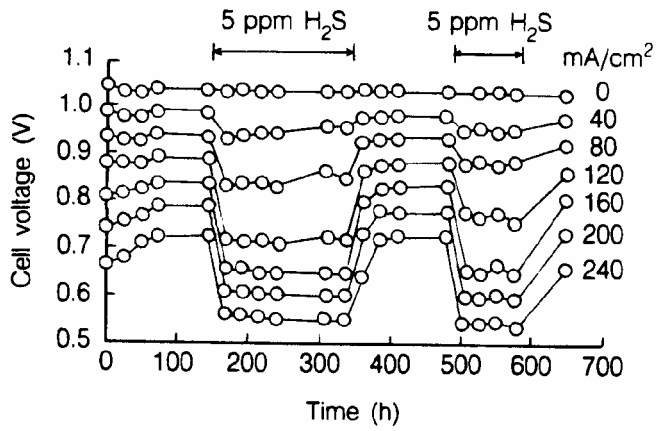

Figure 6-11 Influence of 5 ppm H_2S on the Performance of a Bench Scale MCFC (10 cm x 10 cm) at 650 °C, Fuel Gas (10 percent H_2/5 percent CO_2/10 percent H_2O/75 percent He) at 25 percent H_2 Utilization (78, Figure 4, Pg. 443)

Based on the present understanding of the effect of sulfur on MCFCs, and with the available cell components, it is projected that long-term operation (40,000 hr) of MCFCs may require fuel gases with sulfur[35] levels of the order 0.01 ppm or less, unless the system is purged of sulfur at periodic intervals or sulfur is scrubbed from the cell burner loop (76). Sulfur tolerance would be approximately 0.5 ppm (see Table 6-3) in the latter case. Considerable effort has been devoted to develop low-cost techniques for sulfur removal, and research and development are continuing (80, 81). The effects of H_2S on cell voltage are reversible if H_2S concentrations are present at levels below which nickel sulfide forms.

Halides: Halogen-containing compounds are destructive to MCFCs because they can lead to severe corrosion of cathode hardware. Thermodynamic calculations (82) show that HCl and HF react with molten carbonates (Li_2CO_3 and K_2CO_3) to form CO_2, H_2O, and the respective alkali halides. Furthermore, the rate of electrolyte loss in the cell is expected to increase because of the high vapor pressure of LiCl and KCl. The concentration of Cl^- species in coal-derived fuels is typically in the range 1 to 500 ppm. It has been suggested (83) that the level of HCl should be kept below 1 ppm in the fuel gas, perhaps below 0.5 ppm (47), but the tolerable level for long-term operation has not been established.

***Nitrogen Compounds*:** Compounds such as NH_3 and HCN do not appear to harm MCFCs (70, 79) in small amounts. However, if NO_X is produced by combustion of the anode effluent in the cell burner loop, it could react irreversibly with the electrolyte in the cathode compartment to form nitrate salts. The projection by Gillis (84) for NH_3 tolerance of MCFCs was 0.1 ppm, but Table 6-3 indicates that the level could be 1 vol percent (47).

[35]. Both COS and CS_2 appear to be equivalent to H_2S in their effect on MCFCs (76).

Solid Particulates: These contaminants can originate from a variety of sources, and their presence is a major concern because they can block gas passages and/or the anode surface. Carbon deposition and conditions that can be used to control its formation have been discussed earlier in this section. Solid particles such as ZnO, which is used for sulfur removal, can be entrained in the fuel gas leaving the desulfurizer. The results by Pigeaud (72) indicate that the tolerance limit of MCFCs to particulates larger than 3 μm diameter is <0.1 g/l.

Other Compounds: Experimental studies indicate that 1 ppm As from gaseous AsH_3 in fuel gas does not affect cell performance, but when the level is increased to 9 ppm As, the cell voltage drops rapidly by about 120 mV at 160 mA/cm^2 (71). Trace metals, such as Pb, Cd, Hg, and Sn in the fuel gas, are of concern because they can deposit on the electrode surface or react with the electrolyte (16). Table 6-3 addresses limits of these trace metals.

6.2.5 Effects of Current Density

The voltage output from an MCFC is reduced by ohmic, activation, and concentration losses that increase with increasing current density. The major loss over the range of current densities of interest is the linear iR loss. The magnitude of this loss (iR) can be described by the following equations (64, 85, 86):

$$\Delta V_J(mV) = -1.21\Delta J \qquad \text{for } 50 \leq J \leq 150 \qquad \textit{(6-31)}$$

$$\Delta V_J(mV) = -1.76\Delta J \qquad \text{for } 150 \leq J \leq 200 \qquad \textit{(6-32)}$$

where J is the current density (mA/cm^2) at which the cell is operating.

6.2.6 Effects of Cell Life

Endurance of the cell stack is a critical issue in the commercialization of MCFCs. Adequate cell performance must be maintained over the desired length of service, quoted by one MCFC developer as being an average potential degradation no greater than 2mV/1,000 hours over a cell stack lifetime of 40,000 hours (29). State-of-the-art MCFCs (55, 64, 66, 87, 88) depict an average degradation over time of

$$\Delta V_{lifetime}(mV) = -5mV/1000 \text{ hours} \qquad \textit{(6-33)}$$

6.2.7 Internal Reforming

In a conventional fuel cell system, a carbonaceous fuel is fed to a fuel processor where it is steam reformed to produce H_2 (as well as other products, CO and CO_2, for example), which is then introduced into the fuel cell and electrochemically oxidized. The internal reforming molten carbonate fuel cell, however, eliminates the need for a separate fuel processor for reforming

carbonaceous fuels. This concept is practical in high-temperature fuel cells where the steam reforming reaction[36] can be sustained with catalysts. By closely coupling the reforming reaction and the electrochemical oxidation reaction within the fuel cell, the concept of the internal reforming MCFC is realized. The internal reforming MCFC eliminates the need for the external fuel processor. It was recognized early that the internal reforming MCFC approach provides a highly efficient, simple, reliable, and cost effective alternative to the conventional MCFC system (89). Development to date in the U.S. and Japan continues to support this expectation (85, 90).

There are two alternate approaches to internal reforming molten carbonate cells: indirect internal reforming (IIR) and direct internal reforming (DIR). In the first approach, the reformer section is separate, but adjacent to the fuel cell anode. This cell takes advantage of the close-coupled thermal benefit where the exothermic heat of the cell reaction can be used for the endothermic reforming reaction. Another advantage is that the reformer and the cell environments do not have a direct physical effect on each other. A disadvantage is that the conversion of methane to hydrogen is not promoted as well as in the direct approach. In the DIR cell, hydrogen consumption reduces its partial pressure, thus driving the methane reforming reaction, Equation (6-34), to the right. Figure 6-12 depicts one developer's approach where IIR and DIR have been combined.

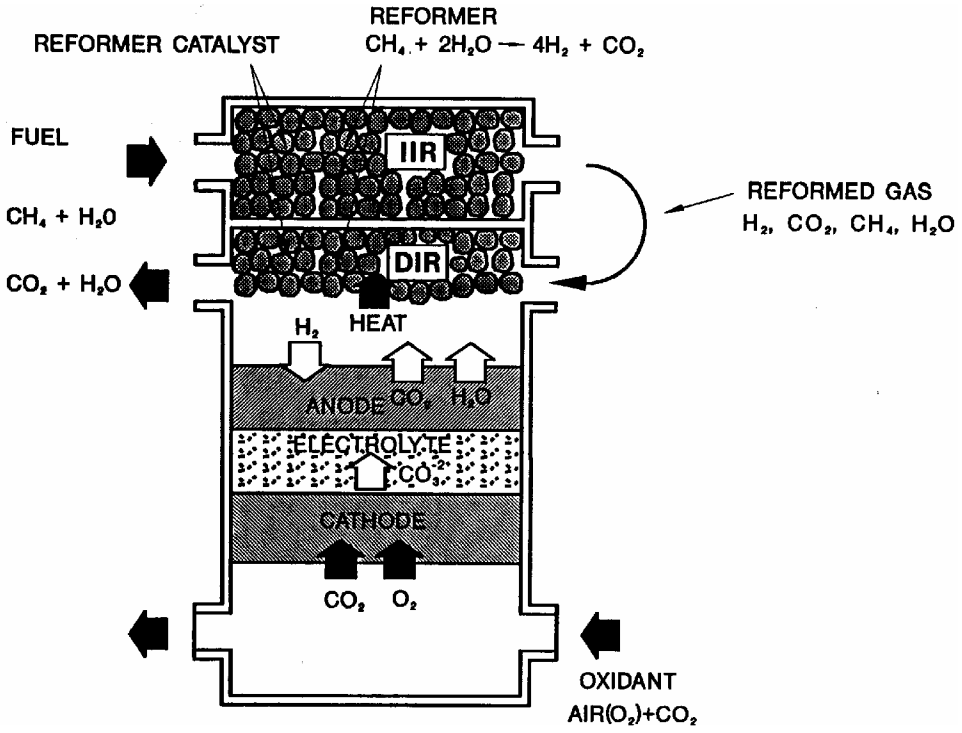

Figure 6-12 IIR/DIR Operating Concept, Molten Carbonate Fuel Cell Design (29)

[36]. Steam reforming of CH_4 is typically performed at 750 to 900 °C; thus, at the lower operating temperature of MCFCs, a high activity catalyst is required. Methanol is also a suitable fuel for internal reforming. It does not require an additional catalyst because the Ni-based anode is sufficiently active.

Methane is a common fuel in internal reforming MCFCs, where the steam reforming reaction

$$CH_4 + H_2O \rightarrow CO + 3H_2 \qquad (6\text{-}34)$$

occurs simultaneously with the electrochemical oxidation of hydrogen in the anode compartment. The steam reforming reaction is endothermic, with $\Delta H_{650°C} = 53.87$ kcal/mol (89), whereas the overall fuel cell reaction is exothermic. In an internal reforming MCFC, the heat required for the reaction in Equation (6-34) is supplied by heat from the fuel cell reaction, thus eliminating the need for external heat exchange that is required by a conventional fuel processor. In addition, the product steam from the reaction in Equation (6-1) can be used to enhance the reforming reaction and the water gas shift reaction to produce additional H_2. The forward direction of the reforming reaction (Equation (6-34)) is favored by high temperature and low pressure; thus, an internal reforming MCFC is best suited to operate near atmospheric pressure.

A supported Ni catalyst (e.g., Ni supported on MgO or $LiAlO_2$) sustains the steam reforming reaction at 650 °C to produce sufficient H_2 to meet the needs of the fuel cell. The interrelationship between the conversion of CH_4 to H_2 and its utilization in an internal reforming MCFC at 650 °C is illustrated in Figure 6-13. At open circuit, about 83 percent of the CH_4 was converted to H_2, which corresponds closely to the equilibrium concentration at 650°C. When current is drawn from the cell, H_2 is consumed and H_2O is produced, and the conversion of CH_4 increases and approaches 100 percent at fuel utilizations greater than about 65 percent. Thus, by appropriate thermal management and adjustment of H_2 utilization with the rate of CH_4 reforming, a similar performance can be obtained in internal reforming MCFC stacks with natural gas and with synthesized reformate gas containing H_2 and CO_2, Figure 6-14. The concept of internal reforming has been successfully demonstrated for more than 15,000 hours in a 5 kW stack (91 and more than 10,000 hours in a 250 kW stack (92) The performance of the 2 kW stack over time can be seen in Figure 6-15 (13).

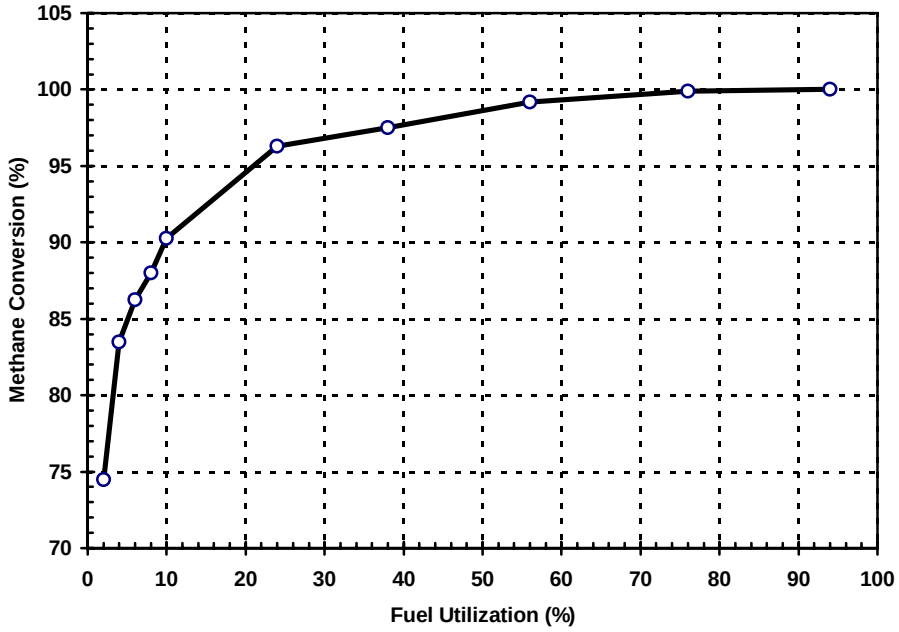

Figure 6-13 CH_4 Conversion as a Function of Fuel Utilization in a DIR Fuel Cell (MCFC at 650 ºC and 1 atm, steam/carbon ratio = 2.0, >99 percent methane conversion achieved with fuel utilization > 65 percent (93)

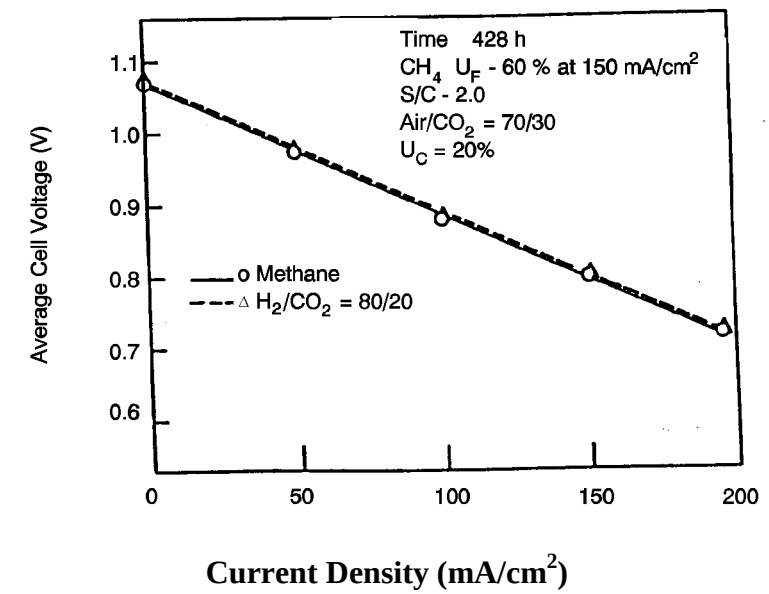

Figure 6-14 Voltage Current Characteristics of a 3kW, Five Cell DIR Stack with 5,016 cm^2 Cells Operating on 80/20 percent H_2/CO_2 and Methane (85)

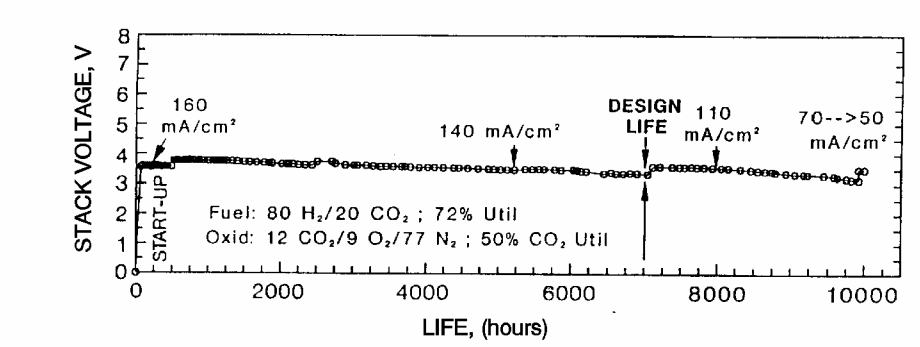

Figure 6-15 Performance Data of a 0.37m^2 2 kW Internally Reformed MCFC Stack at 650 °C and 1 atm (13)

Direct Internal Reforming Catalysts: The anode catalyst is deactivated by the alkali carbonate's electrolyte-containing environment. Making hardware of a non-wetting metal such as nickel has mitigated electrolyte creepage over the hardware surface towards the catalyst. Presently DIR catalyst deactivation is mainly by the vapor phase alkali species. The deactivation mechanism includes electrolyte-accelerated sintering, pore filling/plugging, and surface coverage. Making hardware of a non-wetting metal such as nickel has mitigated electrolyte creepage over the hardware surface towards the catalyst. Alkali-resistant supports such as magnesium oxide, calcium aluminate, and α-alumina have been investigated to reduce vapor phase alkali species effects. Results show that these supports undergo different degrees of decay. Ruthenium and rhodium-based catalysts are more stable, but are too costly (95, 96) FCE has identified a more active and stable DIR catalyst (high activity supported Ni), projecting a catalyst life exceeding 40,000 hours and pursuing further enhancement of catalyst life. Another approach is to apply a getter-type barrier to trap the volatile alkali species before they reach the catalysts. A porous Ni or a SiC membrane was placed between the cell internal catalyst and the electrolyte-containing components. (37)

6.3 Summary of Equations for MCFC

The preceding sections provide parametric performance based on various referenced data at different operating conditions. It is suggested that the following set of equations could be used for performance adjustments unless the reader prefers other data or correlations. Figure 6-16 is provided as reference MCFC performance.

Parameter	Equation	Comments	
Pressure	$\Delta V_p(mV) = 76.5 \log \frac{P_2}{P_1}$	1 atm $\leq$ P $\leq$ 10 atm	(6-19)
Temperature	$\Delta V_T(mV) = 2.16(T_2 - T_1)$	575°C $\leq$ T < 600 °C	(6-21)
	$\Delta V_T(mV) = 1.40(T_2 - T_1)$	600°C $\leq$ T $\leq$ 650 °C	(6-22)
	$\Delta V_T(mV) = 0.25(T_2 - T_1)$	650°C < T $\leq$ 700 °C	(6-23)
Oxidant	$\Delta V_{cathode}(mV) = 250 \log \frac{(\bar{P}_{CO_2}\ \bar{P}_{O_2}^{1/2})_2}{(P_{CO_2}\ P_{O_2}^{1/2})_1}$	$0.04 \leq (\bar{P}_{CO_2}\ \bar{P}_{O_2}^{1/2}) \leq 0.11$	(6-25)
	$\Delta V_{cathode}(mV) = 99 \log \frac{(\bar{P}_{CO_2}\ \bar{P}_{O_2}^{1/2})_2}{(\bar{P}_{CO_2}\ \bar{P}_{O_2}^{1/2})_1}$	$0.11 \leq (\bar{P}_{CO_2}\ \bar{P}_{O_2}^{1/2}) \leq 0.38$	(6-26)
Fuel	$\Delta V_{anode}(mV) = 173 \log \frac{(\bar{P}_{H_2} / \bar{P}_{CO_2}\ \bar{P}_{H_2O}^{1/2})_2}{(\bar{P}_{H_2} / \bar{P}_{CO_2}\ \bar{P}_{O_2}^{1/2})_1}$		(6-27)
Current Density	$\Delta V_J(mV) = -1.21\ \Delta J$	50 $\leq$ J $\leq$ 150mA/cm^2	(6-31)
	$\Delta V_J(mV) = -1.76\ \Delta J$	150 < J $\leq$ 200mA/cm^2	(6-32)
Life Effects	$\Delta V_{lifetime}(mV) = -5mV/1000$ hours		(6-33)

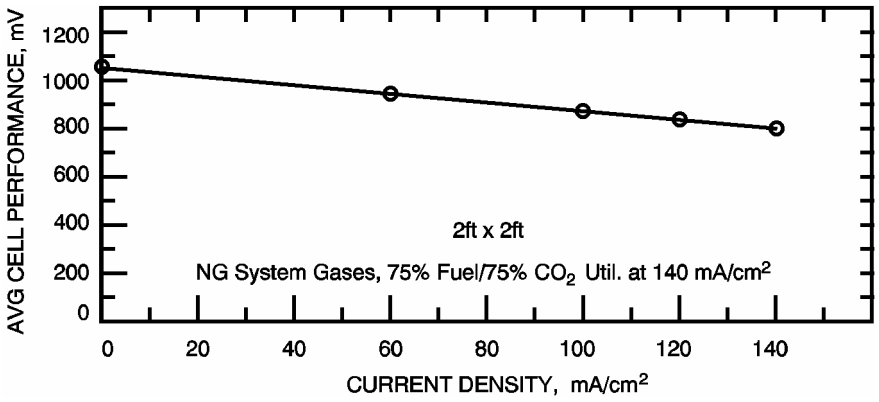

Figure 6-16 Average Cell Voltage of a 0.37m^2 2 kW Internally Reformed MCFC Stack at 650 °C and 1 atm. Fuel, 100 percent CH_4, Oxidant, 12 percent CO_2/9 percent O_2/77 percent N_2

FuelCell Energy presented a computer model for predicting carbonate fuel cell performance at different operating conditions. The model was described in detail at the Fourth International Symposium on Carbonate Fuel Cell Technology, Montreal, Canada, 1997 (97). The model equations are as follows:

The general voltage versus current density relation is:

$$V = E_{Nernst} - (\eta_a + \eta_c) - \eta_{conc} - iz_r \qquad (6\text{-}41)$$

where

$$V_0 = E_0 + \frac{RT}{2F} \ln \left(\frac{P_{H_2,a}}{P_{CO_2,a} P_{H_2O,a}} P_{CO_2,c} \; P_{O_2,c}^{1/2} \right) \qquad (6\text{-}42)$$

At low current density (i<0.04 A/cm^2)

$$\eta_a = \frac{iRT}{2F} \frac{1}{K_a^0} e^{Ea/T} \; p_{H_2}^{\beta-0.5} \; p_{CO_2}^{-\beta} \; p_{H_2O}^{-\beta} \qquad (6\text{-}43)$$

$$\eta_c = \frac{iRT}{2F} \frac{1}{K_a^0} e^{Ec/T} \; p_{CO_2}^{-b_1'} \; p_{O_2}^{-b_2'} \qquad (6\text{-}44)$$

At high current density (i < 0.04A/cm^2)

$$\eta_a = \frac{RT}{2F} \left(a_0 + a_1 \ln p_{H_2} + a_2 \ln p_{CO_2,a} + a_3 \ln p_{H_2O} + a_4/T + a_5 \ln (i) \right) \qquad (6\text{-}45)$$

$$\eta_c = \frac{RT}{2F} \left(b_0 + b_1 \ln p_{CO_2,c} + b_2 \ln p_{o_2} + b_3/T + b_4 \ln i \right) \qquad (6\text{-}46)$$

and

$$\eta = c_6 \ln(1 - i/i_L) \qquad (6\text{-}47)$$

cell resistance

$$Z_r = Z_0 \exp[c(\frac{1}{T_0} - \frac{1}{T})] \qquad (6\text{-}48)$$

A description of the parameters in the model follows:

V	=	Cell voltage, V
E◦	=	Standard E.M.F., V
R	=	Universal gas constant (8.314 joule/deg-mole)
T	=	Temperature, K
P	=	Partial pressure of gas compositions at anode (a) or cathode (c), atm.
η	=	Polarization, V
i	=	Current density, A/cm^2
z	=	Cell impedance, Ω-cm^2
F	=	Faraday's Constant (96,487 joule/volt - gram equivalent)
a,b,c	=	Parameters determined for experiments

The parameters in the above equations were calibrated from 400 sets of FCE's laboratory-scale test data and were further verified by several large-scale stack experiments. These parameter values may depend on the FCE cell design and characteristics, and may not be directly applicable to other carbonate technologies. Figure 6-17 is a comparison of the measured data match with the model prediction.

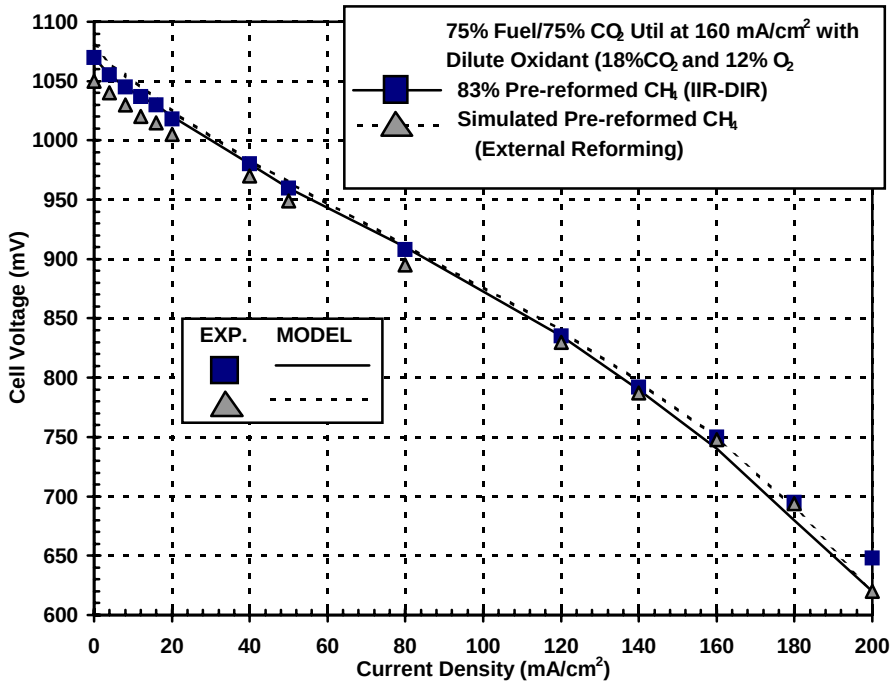

Figure 6-17 Model Predicted and Constant Flow Polarization Data Comparison (98)

6.4 References

1. H.C. Maru, L.G. Marianowski, *Extended Abstracts,* Abstract #31, Fall Meeting of the Electrochemical Society, October 17-22, 1976, Las Vegas, NV, Pg. 82, 1976.R.H.
2. J. Mitteldorf, G. Wilemski, *J. Electrochem. Soc.,* 131, 1784, 1984.
3. R.H. Arendt, *J. Electrochem. Soc.,* 129, 942, 1982.
4. H.C. Maru, A. Pigeaud, R. Chamberlin, G. Wilemski, in *Proceedings of the Symposium on Electrochemical Modeling of Battery, Fuel Cell, and Photoenergy Conversion Systems,* edited by J.R. Selman and H.C. Maru, The Electrochemical Society, Inc., Pennington, NJ, Pg. 398, 1986.
5. H.R. Kunz, *J. Electrochem. Soc.,* 134, 105, 1987.
6. A. Pigeaud, H.C. Maru, L. Paetsch, J. Doyon, R. Bernard, in *Proceedings of the Symposium on Porous Electrodes: Theory and Practices,* edited by H.C. Maru, T. Katan and M.G. Klein, The Electrochemical Society, Inc., Pennington, NJ, Pg. 234, 1984.
7. H.C. Maru, L. Paetsch, A. Pigeaud, in *Proceedings of the Symposium on Molten Carbonate Fuel Cell Technology,* edited by R.J. Selman and T.D. Claar, The Electrochemical Society, Inc., Pennington, NJ, Pg. 20, 1984.
8. R.J. Petri, T.G. Benjamin, in *Proceedings of the 21st Intersociety Energy Conversion Engineering Conference,* Volume 2, American Chemical Society, Washington, DC, Pg. 1156, 1986.
9. R.J. Selman, *Energy,* 11, 153, 1986.
10. M. Farooque, ERC, "Development on Internal Reforming Carbonate Fuel Cell Technology, Final Report," prepared for U.S. DOE/METC, DOE/MC/23274-2941, Pgs. 4-19 - 4-29, October, 1990.
11. FCE correspondence, June 2002
12. R. Huff, "Status of Fuel Cell Technologies," 1986 Fuel Cell Seminar, October 26-29, 1986, Tucson, AZ, 1986.
13. M. Farooque, data from ERC testing, 1992 and 2002.
14. C.E. Baumgartner, V.J. DeCarlo, P.G. Glugla, J.J. Grimaldi, *J. Electrochem. Soc.,* 132, 57, 1985.
15. P.G. Glugla, V.J. DeCarlo, *J. Electrochem. Soc.,* 129, 1745, 1982.
16. C. Yuh, M. Farooque, R. Johnsen, ERC, "Understanding of Carbonate Fuel Cell Resistances in MCFCs," in *Proceedings of the Fourth Annual Fuel Cells Contractors Review Meeting,* U.S. DOE/METC, Pgs. 53 - 57, July, 1992 and FCE correspondence, 2002.
17. C. Baumgartner, *J. Electrochem. Soc.,* 131, 1850, 1984.
18. W.M. Vogel, L.J. Bregoli, H.R. Kunz, S.W. Smith, in *Proceedings of the Symposium on Molten Carbonate Fuel Cell Technology,* edited by R.J. Selman and T.D. Claar, The Electrochemical Society, Inc., Pennington, NJ, Pg. 443, 1984.
19. M.L. Orfield, D.A. Shores, in *Corrosion 86,* Paper No. 88, National Association of Corrosion Engineers, Houston, TX, 1986.
20. D.A. Shores, in *Proceedings of the 22nd Intersociety Energy Conversion Engineering Conference,* Volume 2, American Institute of Aeronautics & Astronautics, New York, NY, Pg. 1023, 1987.
21. Communication with FCE, July 2002.
22. "Development of Improved Molten Carbonate Fuel Cell Technology," Final Report prepared by United Technologies Corp. for the Electric Power Research Institute, Palo Alto, CA, under Contract #RP1085-4, July 1983.

23. T.D. Kaun, in *Proceedings of the Fourth International Symposium on Molten Salts*, edited by M. Blander, D.S. Newman, M.L. Saboungi, G. Mamantov, K. Johnson, The Electrochemical Society, Inc., Pennington, NJ, Pg. 489, 1984.
24. A.J. Appleby, "Advanced Fuel Cells and Their Future Market," *Energy Conservation Strategies*, Progress Series, edited by W.E. Murphy, L.H. Fletcher, American Society of Aeronautics and Astronautics, New York, NY, date unknown.
25. A. Pigeaud, A.J. Skok, P.S. Patel, H.C. Maru, *Thin Solid Films*, 83, 1449, 1981.
26. R.A. Donado, L.G. Marianowski, H.C. Maru, J.R. Selman, *J. Electrochem. Soc.*, 131, 2541, 1984.
27. R.A. Donado, L.G. Marianowski, H.C. Maru, J.R. Selman, *J. Electrochem. Soc.*, 131, 2535, 1984.
28. R.B. Swaroop, J.W. Sim, K. Kinoshita, *J. Electrochem. Soc*., 125, 1799, 1978.
29. M. Farooque, ERC, "Development on Internal Reforming Carbonate Fuel Cell Technology, Final Report," prepared for U.S. DOE/METC, DOE/MC/23274-2941, Pgs.. 3 - 18, October, 1990.
30. D.A. Shores, P. Singh, in *Proceedings of the Symposium on Molten Carbonate Fuel Cell Technology*, edited by R.J. Selman and T. D. Claar, The Electrochemical Society, Inc., Pennington, NJ, Pg. 271, 1984.
31. G. Kucera, K. Myles, A. Brown, M. Roche, D. Chu, E. Indacochea, "ANL's Research and Development of Alternate Components for MCFCs," *in Proceedings of the Fourth Annual Fuel Cells Contractors Review Meeting*, U.S. DOE/METC, July 1992, Pgs. 31 - 41.
32. M Farooque, H.C. Maru, "Carbonate Fuel Cells Overview," *in Proceedings of the American Chemical Society Meeting*, August 2001.
33. N. Minh, "High Temperature Fuel Cells," in *CHEMTECH*, journal published by the American Chemical Society, Vol. 21, No. 1, January, Pgs. 32-37, 1991.
34. Y. Yamamasu, T. Kakihara, E. Kasai, T. Morita, IHI, "Component Development and Durability Test of MCFC," in *The International Fuel Cell Conference Proceedings*, NEDO/MITI, Tokyo, Japan, Pgs. 161-164, 1992.
35. H. Urushibata, T. Murahashi, MELCO, "Life Issues of Molten Carbonate Fuel Cell," in *The International Fuel Cell Conference Proceedings*, NEDO/MITI, Tokyo, Japan, Pgs. 223-226, 1992.
36. S. Takashima, K. Ohtsuka, T. Kara, M. Takeuchi, Y. Fukui, H. Fujimura, Hitachi, "MCFC Stack Technology at Hitachi," in *The International Fuel Cell Conference Proceedings*, NEDO/MITI, Tokyo, Japan, Pgs. 265-268, 1992.
37. C. Yuh, M. Farooque, "Carbonate Fuel Cell Materials," in *Advanced Materials and Processes*, journal published by the American Society of Materials, July, 2002.
38. J. Hirschenhofer, D. Stauffer, R. Engleman, Fuel Cells A Handbook (Revision 3) prepared by Gilbert/Commonwealth, Inc. for the U.S. Department of Energy under Contract No. DE-ACO1-88FE61684, January 1994.
39. K. Tanimoto, Y. Miyazaki, M. Yanagida, S. Tanase, T. Kojima, N. Ohtori, H. Okuyama, T. Kodama, Government Industrial Research Institute, Osaka, "Cell Performance of Molten Carbonate Fuel Cell with Alkali and Alkaline Earth Carbonate Mixtures," in *The International Fuel Cell Conference Proceedings*, NEDO/MITI, Pgs. 185-188, Tokyo, Japan, 1992.

40. K. Ota, S. Mitsushima, K Kato, N. Kamiya, Yokahama National University, "Solubilities of Metal Oxides in Molten Carbonate, " in Proceedings of the Second Symposium on Molten Carbonate Fuel Cell Technology, Volume 90 - 16, The Electrochemical Society, Inc. Pennington, NJ, Pgs. 318-327, 1990.
41. T. Benjamin, et al., "Status of the M-C Power MCFC Commercialization Program," IECEC-97, Honolulu, Hawaii, July 27 - August 1, 1997.
42. A. Yuh, M. Farooque, "Carbonate Fuel Cell Materials," in *Advanced Materials and Processes*, journal published by the American Society of Materials, July, 2002.
43. H. Maru, et al., "ERC Direct Carbonate Fuel Cell Program Overview," DOE Contractor's Review Meeting, Morgantown, WV, August 26-28, 1997.
44. R.O.Petkus, "Successful Test of a 250 kW Molten Carbonate Fuel Cell Power Generator at Miramar," POWER-GEN International '97, Dallas, TX, December 1997.
45. A. Pigeaud, ERC, and G. Wilemski, Physical Sciences, "Effects of Coal-Derived Trace Species on the Performance of Carbonate Fuel Cells," *in Proceedings of the Fourth Annual Fuel Cells Contractors Review Meeting*, U.S. DOE/METC, Pgs. 42-45, July 1992.
46. D. Rastler, EPRI, G. Devore, Destec Engineering, R. Castle, Haldor Topsoe, C. Chi, ERC, "Demonstration of a Carbonate Fuel Cell Stack on Coal-Derived Gas," *in Fuel Cell Seminar.*
47. "Effects of Coal-Derived Trace Species on the Performance of Molten Carbonate Fuel Cells," Topical Report prepared by Energy Research Corporation for US DOE/METC, DOE/MC/25009-T26, October, 1991.
48. A. Pigeaud, et al., "Trace Contaminant Effects and Emissions with Integrated Coal Gasification and Cleanup," 1994 Fuel Cell Seminar, Pgs. 539-542 (1994).
49. L.J. Bregoli and H.R. Kunz, *J. Electrochem. Soc.*, 129, 2711, 1982.
50. Benjamin, et al., "Status of MCFC Technology at M-C Power-1992," 1992 Fuel Cell Seminar Program and Abstracts, 1992.
51. M.G. Gonikberg, *Chemical Equilibria and Reaction Rates at High Pressures,* Translated from Russian by M. Artment, edited by S. Monson, published for the National Science Foundation, Washington, D.C., by the Israel Program for Scientific Translations Jerusalem, Israel, Pg. 58, 1963.
52. M.G. Gonikberg, *Chemical Equilibria and Reaction Rates at High Pressures,* Translated from Russian by M. Artment, edited by S. Monson, published for the National Science Foundation, Washington, DC, by the Israel Program for Scientific Translations, Jerusalem, Israel, Pg. 133, 1963.
53. H.R. Kunz, L.A. Murphy, in *Proceedings of the Symposium on Electrochemical Modeling of Battery, Fuel Cell, and Photoenergy Conversion Systems,* edited by J.R. Selman and H.C. Maru, The Electrochemical Society, Inc., Pennington, NJ, Pg. 379, 1986.
54. T.G. Benjamin, E.H. Camara, L.G. Marianowski, *Handbook of Fuel Cell Performance,* prepared by the Institute of Gas Technology for the United States Department of Energy under Contract No. EC-77-C-03-1545, May 1980.
55. Research and Development on Fuel Cell Power Generation Technology FY1990 Annual Report, NEDO, April 1991.
56. M. Hosalaetal, "IHI Large Site Molten Carbonate Fuel Cell Advancements," *Fuel Cell Program and Abstracts* 1990 Fuel Cell Seminar, Phoenix, AR, November 25-28, 1990.
57. W.H. Johnson, "Molten Carbonate Fuel Cell Technology Improvement," Quarterly Technical Progress Report No. 23 for the Period Ending May, 1990, prepared for US DOE/METC, DOE/MC/23270-2923, September 1990.

58. D.B. Stauffer, et al., "An Aspen/SP MCFC Performance User Block," G/C Report No. 2906, July 1991.
59. J.R. Rostrup-Nielsen, in *Catalysis Science and Technology,* edited by J.R. Anderson and M. Boudart, Springer-Verlag, Berlin, German Democratic Republic, Pg. 1, 1984.
60. H.A. Leibhafsky, E.J. Cairns, *Fuel Cells and Fuel Batteries,* John Wiley and Sons, Inc., New York, NY, Pg. 654, 1968.
61. T.D. Tawari, E. Pigeaud, H.C. Maru, in *Proceedings of the Fifth Annual Contractors Meeting on Contaminant Control in Coal-Derived Gas Streams,* DOE/METC-85/6025, edited by D.C. Cicero and K.E. Markel, U.S. Department of Energy, Morgantown, WV, Pg. 425, January 1986.
62. G.H.J. Broers, B.W. Triejtel, *Advanced Energy Conversion,* 5, 365, 1965.
63. A. Baker, S. Gionfriddo, A. Leonida, H. Maru, P. Patel, "Internal Reforming Natural Gas Fueled Carbonate Fuel Cell Stack," Final Report prepared by Energy Research Corporation for the Gas Research Institute, Chicago, IL, under Contract No. 5081-244-0545, March, 1984.
64. M. Farooque, Data from ERC testing, 1992.
65. S. Kaneko, et al., "Research on On-Site Internal Reforming Molten Carbonate Fuel Cell," 1989 International Gas Research Conference, 1989.
66. M. Farooque, "Development of Internal Reforming Carbonate Fuel Cell Stack Technology," Final Report, DOE/MC/23274-2941, October 1991.
67. J.M. King, A.P. Meyer, C.A. Reiser, C.R. Schroll, "Molten Carbonate Fuel Cell System Verification and Scale-up," EM-4129, final report prepared by United Technologies Corp. for the Electric Power Research Institute, Research Project 1273-1, July 1985.
68. S.H. Lu, J.R. Selman, in *Proceedings of the Symposium on Molten Carbonate Fuel Cell Technology*, edited by R.J. Selman, T.D. Claar, The Electrochemical Society, Inc., Pennington, NJ, Pg. 372, 1984.
69. T. Tanaka, et al., "Research on On-Site Internal-Reforming Molten Carbonate Fuel Cell," 1989 International Gas Research Conference, Pg. 252, 1989.
70. G.L. Anderson, P.C. Garrigan, in *Proceedings of the Symposium on Molten Carbonate Fuel Cell Technology,* edited by R.J. Selman, T.D. Claar, The Electrochemical Society, Inc., Pennington, NJ, Pg. 297, 1984.
71. A. Pigeaud, in *Proceedings of the Sixth Annual Contractors Meeting on Containment Control in Coal-Derived Gas Streams,* DOE/METC-86/6042, edited by K.E. Markel and D.C. Cicero, U.S. Department of Energy, Morgantown, WV, Pg. 176, July 1986.
72. A. Pigeaud, "Study of the Effects of Soot, Particulate and Other Contaminants on Molten Carbonate Fuel Cells Fueled by Coal Gas," Progress Report prepared by Energy Research Corporation for U.S. Department of Energy, Morgantown, WV, under Contract No. DE-AC21-84MC21154, June 1987.
73. V. Jalan, M. Desai, C. Brooks, in *Proceedings of the Symposium on Molten Carbonate Fuel Cell Technology,* edited by R. J. Selman, T. D. Claar, The Electrochemical Society, Inc., Pennington, NJ, Pg. 506, 1984.
74. L.J. Marianowski, *Prog. Batteries & Solar Cells,* 5, 283, 1984.
75. W.V. Vogel and S.W. Smith, *J. Electrochem. Soc.,* 129, 1441, 1982.
76. S.W. Smith, H.R. Kunz, W.M. Vogel and S.J. Szymanski, in *Proceedings of the Symposium on Molten Carbonate Fuel Cell Technology,* edited by R.J. Selman and T.D. Claar, The Electrochemical Society, Inc., Pennington, NJ, Pg. 246, 1984.

77. R.J. Remick, E.H. Camara, paper presented at the Fall Meeting for The Electrochemical Society, Inc., New Orleans, LA, October 7-12, 1984.
78. R.J. Remick, in *Proceedings of the Fourth Annual Contractors Meeting on Contaminant Control in Hot Coal-Derived Gas Streams*, DOE/METC-85/3, edited by K. E. Markel, U.S. Department of Energy, Morgantown, WV, Pg. 440, May 1984.
79. M.C. Williams, D.A. Berry, "Overview of the DOE-Funded Fuel Cell Contaminants R&D Program," Fuel Cell Seminar Program and Abstracts, 1990 Fuel Cell Seminar, Phoenix, AR, November 25-28, 1990.
80. P.S. Patel, S.M. Rich, H.C. Maru, in *Proceedings of the Fourth Annual Contractors Meeting on Contaminant Control in Hot Coal-Derived Gas Streams*, DOE/METC-85/3, edited by K. E. Markel, U.S. Department of Energy, Morgantown, WV, Pg. 425, May 1984.
81. G.L. Anderson, F.O. Berry, G.D. Harmon, R.M. Laurens, R. Biljetina, in *Proceedings of the Fifth Annual Contractors Meeting on Contaminant Control in Coal-Derived Gas Streams*, DOE/METC-85/6025, edited by D.C. Cicero, K.E. Markel, U.S. Department of Energy, Morgantown, WV, Pg. 87, January 1986.
82. T.P. Magee, H.R. Kunz, M. Krasij, H.A. Cole, "The Effects of Halides on the Performance of Coal Gas-Fueled Molten Carbonate Fuel Cell," Semi-Annual Report, October 1986 - March 1987, prepared by International Fuel Cells for the U.S. Department of Energy, Morgantown, WV, under Contract No. DE-AC21-86MC23136, May 1987.
83. G.N. Krishnan, B.J. Wood, G.T. Tong, M.A. Quinlan, in *Proceedings of the Fifth Annual Contractors Meeting on Contaminant Control in Coal-Derived Gas Streams*, DOE/METC-85/6025, edited by D.C. Cicero and K.E. Markel, U.S. Department of Energy, Morgantown, WV, Pg. 448, January 1986.
84. E.A. Gillis, *Chem. Eng. Prog.*, 88, October 1980.
85. T. Tanaka, et al., "Development of Internal Reforming Molten Carbonate Fuel Cell Technology," in *Proceedings of the 25th IECEC*, American Institute of Chemical Engineers, New York, NY, August 1990.
86. M. Miyazaki, T. Okada, H. Ide, S. Matsumoto, T. Shinoki, J. Ohtsuki, "Development of an Indirect Internal Reforming Molten Carbonate Fuel Cell Stack," in the 27th Intersociety Energy Conversion Engineering Conference Proceedings, San Diego, CA, August 3-7, 1992, Pg. 290, 1992.
87. W.H. Johnson, "International Fuel Cells MCFC Technical Accomplishment," in *Proceedings of the Second Annual Fuel Cells Contractor's Review Meeting*, US DOE/METC, May 1990.
88. T. Benjamin, G. Rezniko, R. Donelson, D. Burmeister," IMHEX^{R} MCFC Stack Scale-Up," in the *Proceedings of the 27th Intersociety Energy Conversion Engineering Conference*, Vol. 3, San Diego, CA, Aug. 3-7, 1992, Pg. 290, 1992.
89. H.C. Maru, B.S. Baker, *Prog. Batteries & Solar Cells*, 5, 264, 1984.
90. M. Faroogue, G. Steinfield, H. Maru, "Comparative Assessment of Coal-Fueled Carbonate Fuel Cell and Competing Technologies," in *Proceedings of the 25th IECEC*, Vol. 3, American Institute of Chemical Engineers, New York, NY, 1990.
91. H.C. Maru and M. Farooque, FCE, “Molten Carbonate Fuel Cell Product Design Improvement,” Prepared for U.S. DOE/DARPA, Annual Report, DE-FC21-95MC31184, Pages 5-9, December 1999.
92. H.C. Maru and M. Farooque, FCE, “Molten Carbonate Fuel Cell Product Design Improvement,” Prepared for U.S. DOE/DARPA, Annual Report, DE-FC21-95MC31184, Pages 4-10, December 2000.

93. ERC correspondence, laboratory data, March 1998.
94. M. Farooque, data from ERC testing, 1992
95. S. Katikaneni, C. Yuh, S. Abens and M. Farooque, “Catalysis Today, 2002”.
96. S. Katikaneni, C. Yuh and M. Farooque, “The Direct Carbonate Fuel Cell Technology: Advances in Fuel Processing and Internal Reforming,” ACS Fuel Chemistry, 46(2) 685-688, Preprints, 2001.
97. J. Ding, et al., “A Computer Model for Direct Carbonate Fuel Cells,” Proceedings of the Fourth International Symposium on Carbonate Fuel Cells, 191st Electrochemical Society Meeting, Montreal, May 1997.
98. J. Ding, P. S. Patel, M. Farooque, H. C. Maru, in Carbonate Fuel Cell Technology IV, (eds. J. R. Selman, et al.), The Electrochemical Society, Inc., New Jersey, Pg. 127-138, 1997.